SIMULATION AND CONTROL STRATEGY ADAPTATION OF A PARABOLIC TROUGH COLLECTOR INTEGRATED THERMAL SYSTEM FOR INDUSTRIAL PROCESSES

A THESIS SUBMITTED TO
THE GRADUATE SCHOOL OF NATURAL AND APPLIED SCIENCES
OF
MIDDLE EAST TECHNICAL UNIVERSITY

BY

DENİZ PINARLI

IN PARTIAL FULFILLMENT OF THE REQUIREMENTS
FOR
THE DEGREE OF MASTER OF SCIENCE
IN
MECHANICAL ENGINEERING

JANUARY 2022

Approval of the thesis:

SIMULATION AND CONTROL STRATEGY ADAPTATION OF A PARABOLIC TROUGH COLLECTOR INTEGRATED THERMAL SYSTEM FOR INDUSTRIAL PROCESSES

submitted by **DENİZ PINARLI** in partial fulfillment of the requirements for the degree of **Master of Science** i**n Mechanical Engineering, Middle East Technical University** by,

Prof. Dr. Halil Kalıpçılar
Dean, Graduate School of **Natural and Applied Sciences** _____

Prof. Dr. Mehmet Ali Sahir Arıkan
Head of the Department, **Mechanical Engineering** _____

Assoc. Prof. Dr. Özgür Bayer
Supervisor, **Mechanical Engineering, METU** _____

Examining Committee Members:

Prof. Dr. İlker Tarı
Mechanical Eng., METU _____

Assoc. Prof. Dr. Özgür Bayer
Mechanical Eng., METU _____

Prof. Dr. Derek Keith Baker
Mechanical Eng., METU _____

Prof. Dr. Selin Aradağ Çelebioğlu
Mechanical Eng., TED Uni. _____

Prof. Dr. Hanife Tuba Okutucu Özyurt
Energy Institute, İstanbul Teknik Uni. _____

Date: 11.01.2022

I hereby declare that all information in this document has been obtained and presented in accordance with academic rules and ethical conduct. I also declare that, as required by these rules and conduct, I have fully cited and referenced all material and results that are not original to this work.

Name, Last name : Deniz Pınarlı

Signature :

ABSTRACT

SIMULATION AND CONTROL STRATEGY ADAPTATION OF A PARABOLIC TROUGH COLLECTOR INTEGRATED THERMAL SYSTEM FOR INDUSTRIAL PROCESSES

Pınarlı, Deniz
Master of Science, Mechanical Engineering
Supervisor : Assoc. Prof. Dr. Özgür Bayer

January 2022, 75 pages

In this study, integration of solar heat to a milk pasteurization process is addressed. A single tank system with thermal energy storage (TES) is simulated dynamically by connecting the models of individual components to each other, using a simulation tool coded in Visual Basic. The parabolic trough collector (PTC) model is developed such that the time evolution of temperature distribution along a series of collectors can be observed. Lumped approach is employed in the TES unit model in which the heat transfer fluid (HTF) acts as the storage medium. An on-off control is adapted to the single tank system and the results are presented for the optimized nominal design case. The characteristics and drawbacks of the single-tank system is explored in a parametric analysis. As a result, a two tank architecture is suggested along with PI control of temperature at the collector outlet by mass flow rate modulation. Control strategy is demonstrated in action.

Keywords: Solar Heat For Industrial Processes, Parabolic Trough Collectors, Concentrated Solar Power, Process Heat

ÖZ

ENDÜSTRİYEL PROSESLER İÇİN PARABOLİK GÜNEŞ KOLLEKTÖRLERİ ENTEGRE EDİLMİŞ TERMAL SİSTEMLERE KONTROL STRATEJİ ADAPTASYONU VE SİSTEMİN SİMÜLASYONU

Pınarlı, Deniz
Yüksek Lisans, Makina Mühendisliği
Tez Yöneticisi: Doç. Dr. Özgür Bayer

Ocak 2022, 75 sayfa

Bu çalışmada güneş enerjisinin bir süt pastörizasyon prosesinde kullanılması ele alınmışır. Bu amaç doğrultusunda başta tek tanklı bir sistem önerilmiş ve bileşen modelleri birbirlerine eklemlenerek sistemin zamana bağlı simulasyonu Visual Basic dilinde geliştirilen bir simulasyon aracı ile yapılmıştır. Parabolik güneş kollektörü modeli sıcaklık dağılımının zamana bağlı değişimini gösterir. Isı transferi akışkanının depolama ortamı olarak da kullanıldığı termal enerji depolama ünitesi içindeki sıcaklık dağılımı ihmal edilerek modellenmiştir. Bir aç-kapa kontrol stratejisi tek-tanklı sisteme adapte edilmiş ve bir referans dizayn için sonuçlar sunulmuştur. Tek tanklı sistemin karakteristikleri ve dezavantajları bir parametrik analiz ile keşfedilmiştir. Bu doğrultuda çift tanklı bir sistem bir PI kontrol stratejisi ile birlikte önerilmiştir. Kontrol devresi kollektör çıkışındaki sıcaklığı pompa hızını değiştirerek sabit tutar, performansı çalışmada gösterilmiştir.

Anahtar Kelimeler: Solar Endüstriyel Proses Isısı, Parabolik Güneş Kollektörleri, Konsantre Güneş Enerjisi

This study is dedicated to all researchers around the world who contribute the development of science and engineering for peaceful purposes and brotherhood of nations, to my instructors along the way, to my dear parents, and to
M. Kemal Atatürk

ACKNOWLEDGMENTS

The author wishes to express his deepest gratitude to his supervisor Assoc. Prof. Dr. Özgür Bayer for his guidance, advice, criticism, encouragements and insight throughout the research.

The author would also like to thank the partners in AEE Institute for Sustainable Technologies, Austria (AEE INTEC) for collaboration and sharing the pasteurization heat load profile with METU.

The technical assistance of Mr. Mustafa Yalçın is gratefully acknowledged.

This work is partially funded by Integrating National Research Agendas on Solar Heat for Industrial Processes under grant number H2020-731287.

TABLE OF CONTENTS

LIST OF TABLES

TABLES

LIST OF FIGURES

FIGURES

LIST OF ABBREVIATIONS

ASHRAE	American Society of Heating, Refrigerating and Air Conditioning Engineers
AEE INTEC	AEE – Institute for Sustainable Technologies
CFL	Courant Friedrichs Lewy Number
CPC	Compound Parabolic Collector
DNI	Direct Normal Irradiation
EES	Engineering Equation Solver
EJ	Exajoules
EN	European Standards
ETC	Evacuated Tube Collector
FPC	Flat Plate Collector
FVM	Finite Volume Method
HCE	Heat Collector Element
HEX	Heat Exchanger
HTF	Heat Transfer Fluid
IAM	Incidence Angle Modifier
IEA	International Energy Agency
INSHIP	Integrating National Research Agendas on Solar Heat for Industrial Processes
IST	International Solar Technology
IPH	Industrial Process Heat
KPI	Key Performance Indicator
LS	Luz Solar Industries
MERRA	Modern Era Retrospective Analysis for Research and Applications
MS	Microsoft
N/A	Not Applicable
NREL	National Renewable Energy Laboratory

ORC	Organic Rankine Cycle
PDE	Partial Differential Equation
PID	Proportional Integral
PTC	Parabolic Trough Collector
RMSE	Root Mean Square Error
SEGS	Solar Electricity Generating System
SHIP	Solar Heat for Industrial Processes
SIPH	Solar Industrial Process Heat
SPH	Solar Process Heat
STE	Solar Thermal Electricity
TES	Thermal Energy Storage
TMY	Typical Meteorological Year
VBA	Visual Basic for Applications

LIST OF SYMBOLS

Latin Symbols

A	Area
Bi	Biot Number
D	Diameter
E	Energy
Fo	Fourier Number
H	Height
K	Control constants
L	Length
N	Number
Pe	Peclet number
PI	Proportional Integral control
Re	Reynold's number
T	Temperature
U	Overall heat transfer coefficient
Q	Heat transfer
$\dot{Q}$	Heat transfer rate
$\dot{Q}'$	Heat transfer rate per unit length
V	Volume | Velocity
W	Width
c	Specific heat | constant
d	Differential
f	Darcy's friction factor
h	Specific Enthalpy
$\dot{m}$	Mass flow rate
$\dot{m}''$	Mass flow rate flux
t	Time

u	Specific Internal energy
x	Spatial position

Greek Symbols

Δ	Finite difference
Φ	Solar zenith angle
α	Thermal diffusivity
δ	Declination
ε	Surface roughness
η	Efficiency
μ	Dynamic viscosity
ν	Kinematic viscosity
ρ	Density
θ	Solar incidence angle
ω	Solar hour angle

LIST OF SUBSCRIPTS

0	0^{th} control volume | numbering
D	For characteristic length of diameter
ap	Aperture
abs	Absorbed
amb	Ambient
avg	Average
c	Cross-sectional
col	Collectors
end	At collector outlet
i	i^{th} control volume | integral constant
ht-amb, col	Heat transfer to the ambient from collector side
ht-amb, tank	Heat transfer to the ambient from storage tank side
nom	Nominal
opt, 0°	Optical at zero incidence angle
p	At constant pressure | proportional constant
pp	Pinch point
pump, out	Pump outlet
ref	Reference
res	Residual
sr	Series

CHAPTER 1

INTRODUCTION

1.1 Background

Industrial process heat (IPH) is defined as the thermal energy used directly in the preparation or treatment of materials to produce manufactured goods [1]. IPH is vital for the industrial sectors such as food, dairy, textile, paper, chemical, pharmaceuticals, automobile, rubber, steel, cement, and many others [2]. There is a total of 85 EJ (1 EJ = 10^{18} Joules) yearly IPH demand worldwide out of 360 EJ of the world's total energy consumption [3]. In Figure 1.1, the share of IPH in the world's total energy consumption is visualized; in addition, the share of resources of IPH, processes where IPH is used, and classification by temperature ranges are presented. Figure 1.1 clarifies that IPH demand is mainly supplied by fossil-fuel-based resources, creating air pollution, greenhouse gas emissions, and sustainability issues. To reduce these negative environmental impacts, the share of renewables must be increased. Among the renewable resources, solar energy has great potential. Theoretically, only 0.1% of the solar energy available on earth is enough to supply four times the world's total energy demand at a 10% efficiency [4]. Once properly harvested, solar energy can be used to produce IPH. The utilization of solar energy to generate IPH is referred to as Solar Heat for Industrial Processes (SHIP, also known as SIPH or SPH).

Besides its advantages of sustainability, low operating cost, and small environmental impact, there are also challenges involved. Due to the dynamic nature of solar irradiation, TES and auxiliary heater units are required in most systems. The systems already installed in the facilities are not standardized, and casewise expertise is required to integrate the solar heating system into the existing one [5].

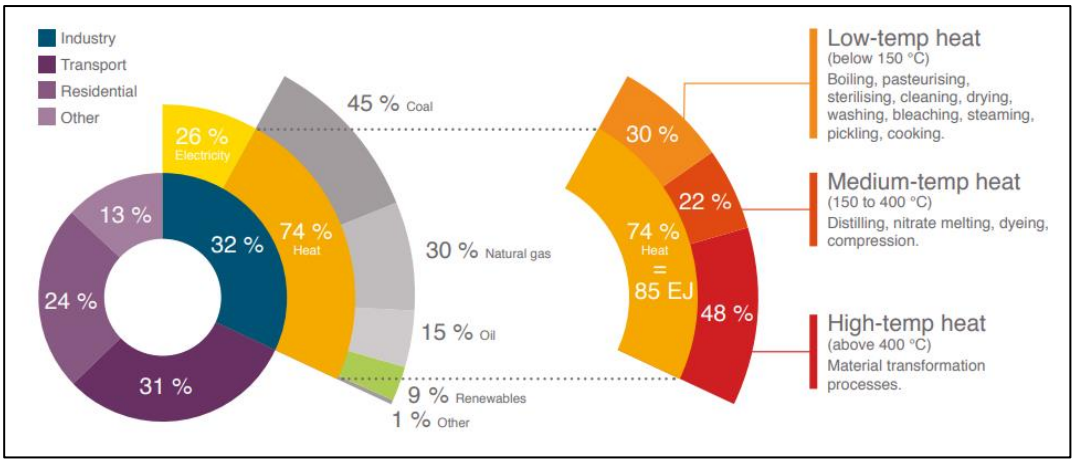

Figure 1.1. Statistics, resources, related processes, and classification by temperature ranges of worldwide IPH demand [6].

Frequently the problem of multiple processes demanding IPH at different temperatures is encountered, which makes the integration more complicated. Also, load profiles depend on the industrial facility's processes, scale, and shifts. As a result, heat load profiles of many industrial sites are rendered time dependent. The payback period of SHIP systems is 6-8 years, affecting the levelized cost of solar thermal energy negatively [7–9]. The SHIP system's collector field either occupies land or requires the facility's roof to be free and structurally robust. Some concentrating solar collector technologies lack roof-mounted variants. To sum up, it is evident that SHIP has great potential; however, more development and cost reduction are required, especially on the solar collectors, to realize this potential to the full. Projects such as IEA Task 49, INSHIP, Solar Twins are funded to remove barriers in front of SHIP in integration and technology.

In SHIP applications, solar collectors convert solar irradiation into useful heat. A suitable collector type should be selected for an application such that the operating temperature of the collector is at least 5-10 °C more than the temperature requirement of the process [10–16]. Maximum operating temperature ranges and commonly used processes for different types of solar collector technologies are given in Figure 1.2.

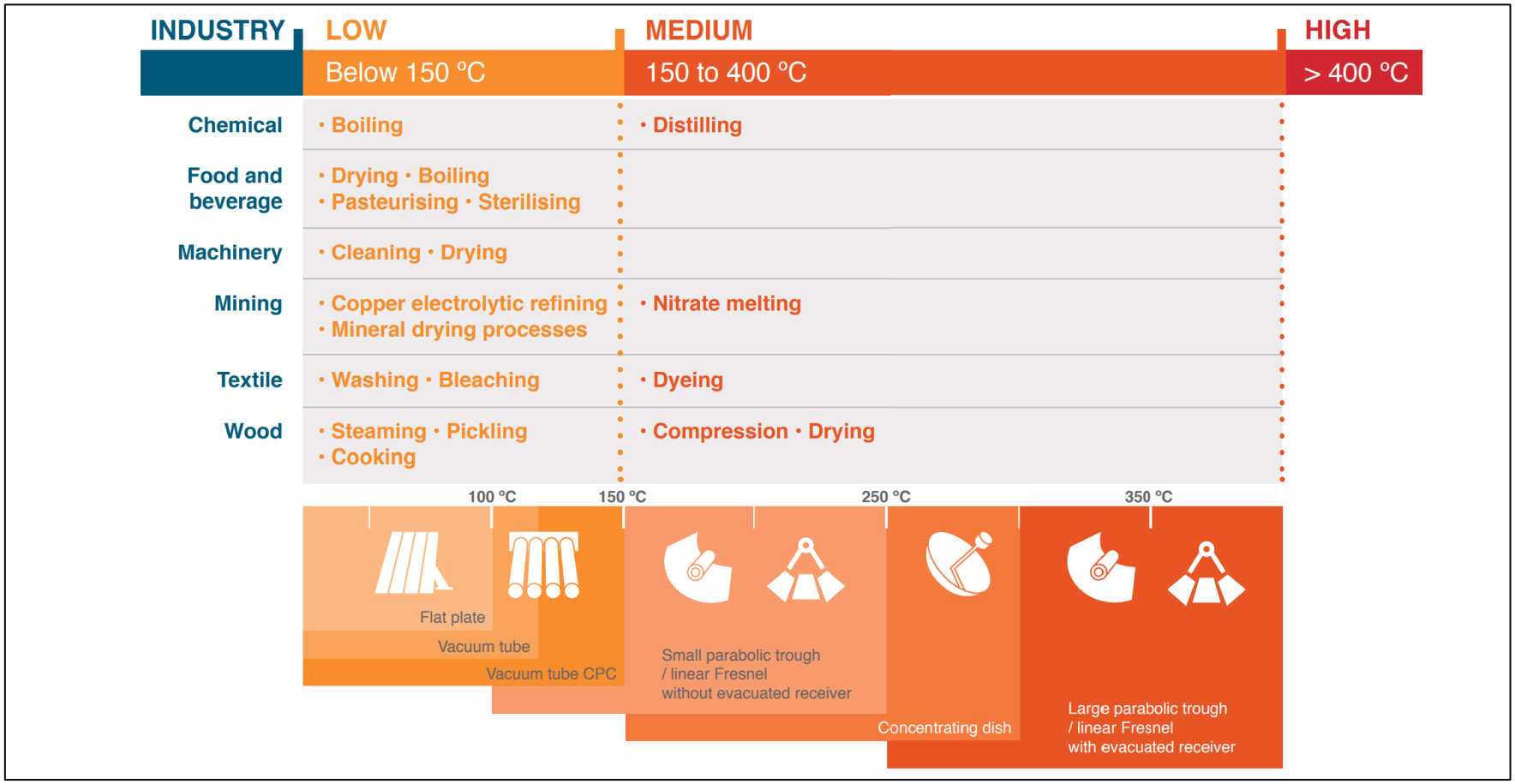

Figure 1.2. Typical operating temperature ranges of solar collector technologies and most commonly used processes [17].

Solar collectors can be classified into two categories as being concentrating and non-concentrating. Among the types shown in Figure 1.2, flat plate and vacuum tube types are non-concentrating, and all the other types are concentrating. In concentrating collectors, the sun rays falling onto the concentrator aperture are directed towards the receiver surface with a significantly smaller surface area. The ratio of the concentrator aperture area to the receiver surface area is called the concentration ratio. The concentration ratio significantly impacts the maximum attainable temperature of a type of solar collector technology. While temperatures up to ~100°C are attainable by non-concentrating collectors, the 100-400°C range requires the usage of concentrating collectors. Due to the Heat Transfer Fluid (HTF) degradation [18], none of the commercially available collectors can exceed the 400°C limit by the time of writing. Concentrating collectors can further be classified into two categories, considering whether the rays are concentrated onto a point or a line. Among the types shown in Figure 1.2 parabolic dish type falls into the category of point focusing, and all other concentrating types in Figure 1.2 fall into the category of line focusing systems. While all types of technologies in Figure 1.2 have the direct flow variants, Flat Plate Collector (FPC), Evacuated Tube Collector (ETC), and Compound Parabolic Collector (CPC) types also have variants in which the solar irradiation is collected utilizing a heat pipe. All direct flow and line focusing types of solar collectors have one component in common; that is, a receiver pipe (also known as absorber pipe or absorber tube) through which an HTF is circulated. And, the receiver pipe is, in fact, a tubular heat exchanger. Thus, tubular heat exchanger theories can be used in the development of a thermo-fluid model of an HTF flow in a solar collector's receiver pipe.

The statements above points out that development of a flexible simulation tool is worthwhile to address performance estimation and feasibility. It is desirable to run simulations for a generic low-medium temperature SHIP system, at any location, having any tubular heat exchanger type of collectors in its solar field, for any time dependent process-heat load profile. According to the results it may be proceeded

forward with system architecture optimization and control strategy adaptation for a particular system to further improve the performance.

For the specific application presented in this study, PTC technology is selected due to its ability to attain the temperature required by the process and the modularity of individual units; although, the methodology can also be applied to previously mentioned collector types with minimal effort.

1.2 Literature Review

The literature on standalone PTC models, complete SHIP plant simulations, control of solar systems, and process integration options are reviewed in this title. All these topics touch on different aspects of the present study.

An individual PTC is the smallest unit in the collector field of a SHIP plant. It is essential to employ a PTC model to develop a complete SHIP plant model. Given the operating conditions, a PTC model estimates the useful solar heat transferred to the HTF. Experimental models are described in American Society of Heating, Refrigerating and Air Conditioning Engineers – 93 (ASHRAE93) steady-state (0D) and EN12975-2 quasi-dynamic (0D) test methods [19]. Commercial collectors are incorporated into these standardized tests, and the coefficients in the experimental correlations are determined by regression analysis. In the early 90s, Dudley et al. tested Solar Electricity Generating System (SEGS) LS-2, SEGS LS-3, ACUREX 3001-03, and International Solar Technology (IST) collectors in Sandia National Laboratories and reported the results [20–22]. From the 2000s on, numerical heat transfer analyses started appearing in literature, and Dudley's test results are extensively referred to for verification [23–29]. Increasingly detailed numerical analyses are conducted that obtained closer results to the experimental data.

The trend was started with Forristal's pioneering study, presented in an National Renewable Energy Laboratory (NREL) technical report in 2003 [30]. He conducted

a steady 0D and a more accurate steady 1D heat transfer analysis of Heat Collector Element (HCE) using Engineering Equation Solver (EES) and compared the results. The comparison revealed that using the 1D model makes 0.5% difference in solar heat gain and efficiency and a 5% to 10% difference in heat transfer to ambient for ~780 meters of receiver length. On the other hand, the 1D model was less flexible, required longer iteration time, and had difficulties converging. Forristal's results were reasonably accurate, with a maximum Root Mean Square Error (RMSE) of 1.56% in collector efficiency. Therefore, his modeling approach is employed with minor differences in several studies [26,31,32]. This approach includes using Gnielinski correlation [33] to obtain the Nusselt number of the flow in the receiver pipe, calculating the convection coefficient between the receiver pipe and the glass cover when the pressure in the annulus is less than 0.013 pascals by Ratzel's study [34], estimating the convective heat transfer between the receiver pipe and the glass cover when the pressure in the annulus is more than 0.013 pascals by Raithby and Holland's correlation [35]. The approach further includes assumption of the receiver pipe and glass cover surfaces as diffuse-gray-isothermal surfaces to determine the radiative heat transfer, using Churchill and Chu's correlation [36] to estimate the convective transfer from the glass cover to the ambient air when there is no wind, calculating the convective heat transfer to the ambient air by Zhukauskas' correlation [37] when there is wind, modeling the radiative heat transfer from the glass cover to the surroundings as if the radiative transfer is taking place between a gray-diffuse-isothermal body and the sky as a blackbody at a temperature 8°C less than the ambient temperature.

Garcia-Valladares et al. introduced a 1D transient analysis of a standard single-pass HCE to explore the impact of the double-pass case [24]. Unlike Forristal's analysis, in [24], the receiver pipe is included in the discretized domain. As a result, an iterative algorithm is used to solve the coupled energy equations. Despite the increased complexity, Garcia et al. obtained less accurate results compared to Forristal's in some cases. Later on, Padilla et al. improved Garcia's analysis by further including the glass cover into the discretized domain and taking conduction

heat transfer to the support brackets into account [23,25]. Discretizing the glass cover led view factor calculations to be involved in the problem and made summations appear in the radiative transfer terms. Padilla et al. presented more accurate results for LS-2 collector compared to both Forristal's and Garcia's results except for the black chrome coating with air in the annulus case. The maximum RMSE between the experimental data and Padilla's outputs is 1.23%. Besides estimating the solar heat transferred to the HTF, the thermal analysis studies mentioned above aim to explore the heat transfer phenomenon taking place in PTCs in detail.

PTC models are also employed as plant models in control tools. The purpose for the issue is to control the HTF temperature at the collector field outlet. Time delays are added to experimental 0D steady models to take into account the traveling time of HTF through the length of a series of PTCs [38]. 1D transient models are proposed as they capture the transient response of the plant, namely the PTC. Camacho et al. suggested a 1D transient model in which both the HTF and the receiver pipe metal are included in the discretized domain [39]. Although similarities between [24] and [39] are present, the heat transfer to ambient model in [39] is significantly more straightforward. In [24], each iteration requires four steps to obtain consistent temperatures; whereas, in [21], an iteration is completed in two steps. The model in [39] can be regarded as a fairly complicated one among the PTC models employed for control purposes.

Although numerical solutions are needed for complex models, analytical approaches for PTC modeling are also available in some cases. The governing equation of the 1D transient model for the HTF domain is an inhomogeneous hyperbolic Partial Differential Equation (PDE). The analytical solution to this problem is presented in [40]. However, the integral appearing in the solution due to the inhomogeneity needs to be performed numerically in most cases. Bayer et al. suggested a semi-analytical solution to the PDE for time-independent boundary conditions, using the Lagrangian description [41], and further compared the suggested solution to the finite volume-based method. The comparison revealed that the semi-analytical solution reduces the computation time significantly without compromising accuracy.

On the other end of the range stand 3D PTC models, studied using commercial software such as ANSYS and Solidworks [27–29,42,43]. Numerical solutions of these models give great detail, but they are computationally expensive. In [28,29,42] 3D and steady models are presented; whereas, both steady and transient analyses are conducted in [27]. In [27], the transient response of a PTC is simulated for 24 hours, with a mesh having 3872 nodes.

While PTC models focus on an isolated, standalone collector, complete SHIP simulations are also available in the literature [5,8,11,44–50]. Comparison of two systems with and without a TES unit in [45] revealed that the presence of a Thermal Energy Storage (TES) unit significantly increases the solar fraction on clear days. In [46], it is revealed that taking the heat transfer from piping to the ambient of a solar farm into account has a marginal impact on the solar field efficiency. For an HTF temperature of 150°C, even for the uninsulated pipe with an overall heat transfer coefficient of 10 W m^{-2} K^{-1}, the efficiency deviates by 1.5%. Transient simulation tools such as TRNSYS, Dymola and Modelica are used in [5,46,48]. The tools provide a simulation environment in which related parameters of system components can effortlessly be connected to each other. However, it is not possible or impractical to construct a 1D model using these softwares. Continuous or piecewise continuous load profiles at constant temperature are inspected in [5,8,44–48]. Off-times on weekends and off-times on hourly periods are addressed; although time dependence of load temperature is not in literature. A new tool is under development to compile factory heat load profiles on a database [51].

Control of solar systems are extensively studied in literature with the purpose of controlling the temperature at the collector field outlet in electricity generation systems [52–66]. While many alternatives including Proportional Integral Derivative (PID), fuzzy logic, model predictive and neural network controllers are suggested for high temperature Solar Thermal Electricity (STE) systems, for SHIP applications relatively more straightforward algorithms such as Proportional Integral (PI) and on-off control are suggested [13,67]. A control strategy for solar system supplying heat to multiple processes is suggested in [12,13,68]. Supplying heat from a single tank

system, in [13], solely on-off control is adapted for the solar pump. In [12,68] pumps on the process side are on-off controlled to direct the stored HTF to the selected process such that thermal energy is most effectively utilized. On-off and PI control are compared for an ETC integrated SHIP system with single stratified storage unit in [67]. The comparison revealed that solar heat gain is increased by 12% when PI control is implemented. Transfer functions for solar collectors are investigated in [69–71]. The transfer functions are found out to be non-linear, and linearization around an operating point is conducted.

System architecture alternatives and integration options are covered in [16,72–76]. Classification by the phase of heat transfer medium in the solar loop side and classification by the process-side-heat-exchanger type are handled [16,74]. The combinations of direct and indirect solar heating of storage medium, single tank, and two tank systems are presented. Thermal energy storage options are mentioned including sensible pressurized or non-pressurized fluid, sensible solid, latent, and chemical alternatives. The steps to be followed for integration are given in [16,74,76]. It is suggested to start with a generic system according to the classification and to keep developing the system architecture, control strategy, and process integration in a loop. Information about existing applications is presented in [75,77] and the online database [78].

1.3 The Present Study and Thesis Organization

In the present study, integration of solar heat to a milk pasteurization facility in Graz, Austria is investigated. The case of the milk pasteurization load temperature being time dependent is addressed. Within the scope of Integrating National Research Agendas on Solar Heat for Industrial Processes (INSHIP) project the heat load profile presented in Table 1.1 is made available to METU by the project partner AEE – Institute for Sustainable Technologies (AEE-INTEC). Following the integration procedures in [16,74,76], a simulation tool is used to estimate the performance of a single-storage-tank system suggested in [16] with a rather simple

control strategy. A nominal case input set is generated methodologically as reference values, and a parametric analysis is conducted around the reference values. Based on the conclusions drawn from the parametric analysis an alternative system architecture is suggested with a more complex control algorithm. Although cost is not taken under consideration in this study, effective usage of collectors is concerned.

Table 1.1 The daily heat load profile of the milk pasteurization facility under investigation in the summer season

Time Interval [hh:mm]	Load Temperature [°C]	Process Load [kW]
10:30 – 12:00	85	293.22
12:00 – 14:30	74	
14:30 – 15:30	40	
15:30 – 19:00	74	

The development of the simulation tool was first started with the 1D-transient thermo-fluid modeling of an HTF flow in a PTC receiver pipe. It is desirable to obtain the transient temperature distribution along a series of collectors from the control point of view. Hence the 1D HTF flow model is employed, and the development is carried out in Visual Basic for Applications (VBA) language in Microsoft (MS) Excel environment. The tool is then upgraded such that it can run complete system simulations for any tubular HEX type of collector, any time dependent load profile, and used for the specific application of the present study.

The single-tank system and the modeling of components are addressed in chapter 2. The simulation tool inputs, outputs, Key Performance Indicators (KPI), and the program flow are introduced along with the nominal case in chapter 3. The methodology followed in determining the nominal case inputs, simulation results, and validation are also given in chapter 3. In chapter 4, the parametric analysis is conducted, and improvements in plant architecture are suggested, along with control strategy alternatives.

CHAPTER 2

SHIP PLANT MODELING

2.1 SHIP Plant Description

The modeled system illustrated in Figure 2.1 is composed of a PTC field, a TES unit, a gasketed-plate type heat exchanger, pumps, valves, fittings, and piping. To achieve maximum utilization of the collector field area, the PTC technology is selected among various collector types due to its sun-tracking ability, superior performance, and efficiency [5]. Specifically, PowerTrough 110 by Inventive Power is selected for the current application [79]. The maximum operating temperature of PowerTrough 110 is given as 130°C under 900 W m^{-2} solar irradiation at zero incidence angle. The peak load temperature of the process is given as 85°C. As previously mentioned at least 5-10°C of pinch point temperature difference between the HTF and the load is recommended. Taking the non-ideal operating conditions into account, the operating temperature range of the selected PTC seems reasonable. North-South axis tracking mode is employed as it is advantageous compared to East-West mode in the summer season [80,81]. A system with TES is preferred as it is desirable to undertake the load using stored solar energy when direct solar radiation is unavailable. Pressurized water is selected as the HTF to prevent phase change during the operation. The HTF is also used as the sensible heat storage medium. It can directly be pumped to the gasketed-plate type heat exchanger.

To obtain a model of the described plant, sub-models of individual plant components are developed and connected to each other. In the following titles, these sub-models are presented. In section 3.8, the model is validated by comparison of the present study results with other study's in literature.

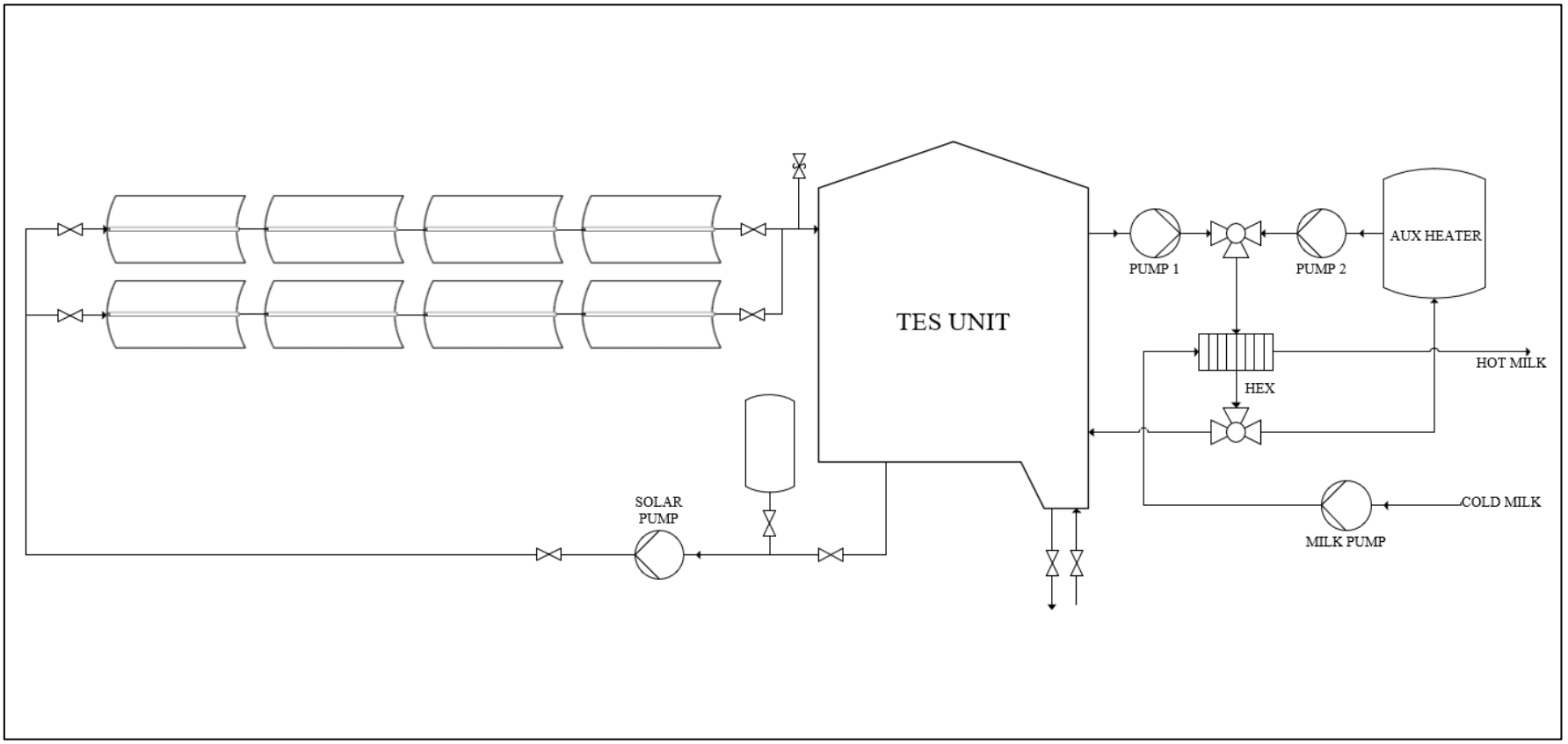

Figure 2.1. Modeled single-tank milk pasteurization SHIP plant

2.2 PTC Field Model

PTC field is the largest component in the SHIP plant. It is composed of a number of individual PTCs connected in series and in parallel. The collector field performance is heavily dependent on the individual collector's performance. A series of collectors are considered together in the thermal model.

2.2.1 The HTF Thermo-fluid model in PTC Receiver Pipe

The HTF flow in the PTC receiver pipe is modeled as uniform, incompressible, single-phase, and turbulent. Temperature is assumed to be uniform in a cross-section and considered as a function of longitudinal position, x, and time, t. Hence, the thermal model is 1D and transient. Absorbed solar radiation and heat transfer to the ambient are treated as they are imposed uniformly on the circumference. Axial conduction is neglected compared to convection effects; since, the Peclet number ($Pe_D = VD/\alpha$) is large ($Pe_D > 100$). The mass and energy interactions of the disc-shaped differential control volume in the PTC receiver pipe are illustrated in Figure 2.2.

The energy equation for the differential control reads:

$$\dot{m}\,[h(x,t) - h(x+dx,t)] + \left(\dot{Q}'_{abs} - \dot{Q}'_{ht-amb,col}\right) dx = \rho\, A_c\, dx\, \frac{\partial u(x,t)}{\partial t} \qquad \text{Eq. (2.1)}$$

After some manipulations, Equation 2.1 can be written in the form:

$$\frac{\partial u(x,t)}{\partial t} + V\, \frac{\partial h(x,t)}{\partial x} = \frac{\dot{Q}'_{abs} - \dot{Q}'_{ht-amb,col}}{\rho\, A_c} \qquad \text{Eq. (2.2)}$$

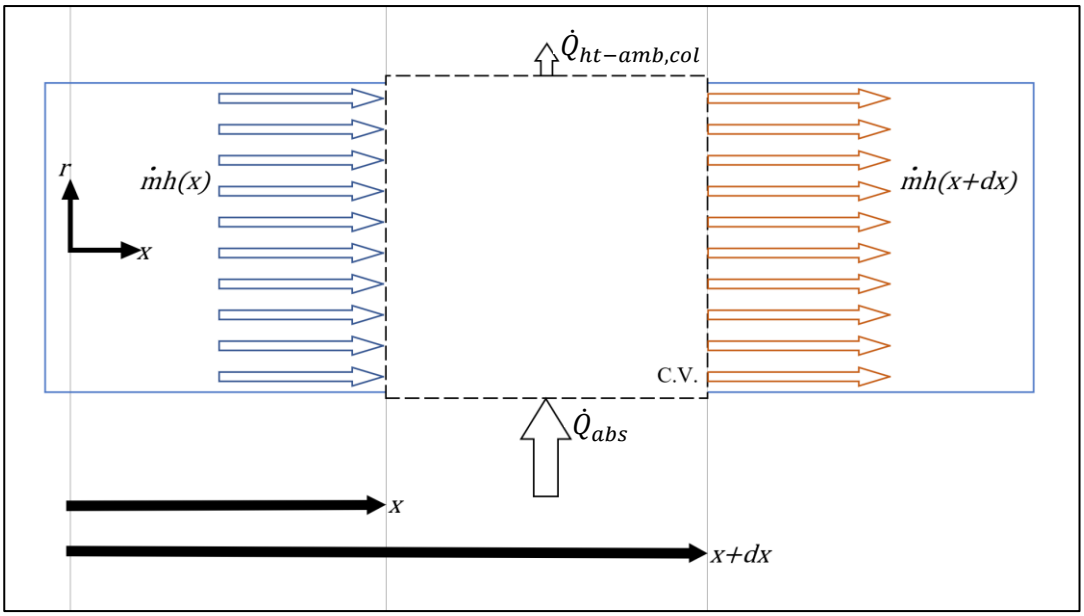

Figure 2.2. Mass and energy interactions of the differential control volume in the cross section of a receiver pipe

Assuming constant material properties, Equation 2.2 simplifies to:

$$\frac{\partial T(x,t)}{\partial t} + V\,\frac{\partial T(x,t)}{\partial x} = \frac{\dot{Q}'_{abs} - \dot{Q}'_{ht-amb,col}}{\rho\, c_p\, A_c} \qquad \text{Eq. (2.3)}$$

Equation 2.3 is an inhomogeneous hyperbolic PDE. The inhomogeneity stems from the forcing term on the right-hand side. It is subjected to the uniform initial condition $T(x, t = 0) = T^0$. The boundary condition $T(x = 0, t) = T_0(t)$ is imposed at the collector inlet. Neglecting the traveling time and heat transfer of the HTF to ambient in the piping, temperature at the pump exit is given as the inlet boundary condition, $T_0(t) = T_{pump,out}(t)$, to the collectors in series.

To prevent the collector field from cooling the HTF, the parameter V in equation 2.3 is conditionally determined by the following relation:

$$V = \begin{cases} 0, & \dot{Q}_{abs} < \dot{Q}_{ht-amb,col} \\ V_{nom}, & \dot{Q}_{ht-amb,col} \leq \dot{Q}_{abs} \end{cases} \quad \text{Eq. (2.4)}$$

The event of $\dot{Q}_{abs}$ being smaller than $\dot{Q}_{ht-amb,col}$ may take place in two ways. First, during the sunrise and the sunset, there is an interval in which the solar irradiation intensity is not sufficient to heat up the HTF. Second, when the temperature at the collector outlet exceeds the maximum operating temperature of the PTC. Setting the pump off, in this case, prevents HTF from cooling while defocusing the receiver protects the collectors.

In the following sections, calculations of $\dot{Q}_{abs}$ and $\dot{Q}_{ht-amb,col}$ are explained.

2.2.1.1 Calculation of Absorbed Solar Radiation

To calculate the absorbed solar radiation, the solar incidence angle for a location and time must be determined. Once the solar incidence angle is determined, it is further modified by the Incidence Angle Modifier (IAM). Collector end losses are neglected. Absorptivity of the receiver pipe, transmissivity of the glass cover, reflectivity, and intercept of the mirror are taken into consideration in the optical efficiency parameter, $\eta_{opt,0^\circ}$. Absorbed solar radiation for PowerTrough 110 is calculated as follows:

$$\dot{Q}_{abs} = \eta_{opt,0^\circ} A_{ap} \, (DNI) \, \cos(\theta) \, IAM(\theta) \quad \text{Eq. (2.5)}$$

where the optical efficiency at zero incidence angle, $\eta_{opt,0^\circ}$, is experimentally measured as 0.6 and the surface area of collector aperture, A_{ap}, is 3.36 m^2.

2.2.1.1.1 The Solar Incidence Angle

The solar incidence angle for a PTC is the angle between the solar rays and the concentrator aperture plane's surface normal. It depends on the location, solar time, and the tracking mode of the collector. Calculation of the solar time and the solar incidence angle for commonly encountered surfaces is a foundational problem in solar energy and comprehensively addressed in textbooks [80,81]. While the complete procedure can be followed from the referenced resources, the final formula is presented here. The solar incidence angle for N-S tracking mode is obtained by the formula [80]:

$$\theta = \text{acos}\left(\cos(\delta)\sqrt{sin^2(\omega) + \left(\cos(\Phi)\cos(\omega) + \tan(\delta)\sin(\Phi)\right)^2}\right) \quad \text{Eq. (2.6)}$$

2.2.1.1.2 Incidence Angle Modifier

The PTC design is based on the zero-incidence angle design point. Any solar incidence angle other than 0° leads to less available solar radiation at the aperture. However, PTCs perform even poorly under non-zero incidence angles. The IAM is introduced as a factor between zero and one to take these effects into account. IAM always reads one at zero incidence angle for all PTCs, while it goes to zero around 75° incidence angle for most PTCs.

While IAM relations for large PTCs are presented in detail in test reports, IAM correlation of small PTCs, including PowerTrough 110, are often unavailable in the datasheets. Nevertheless, the procedure is continued with the following suggested model that captures common trends for IAM:

$$IAM(\theta) = \begin{cases} 1 - \dfrac{0.1}{30}\theta, & 0 \le \theta < 30° \\ 0.9 - \dfrac{0.3}{30}(\theta - 30°), & 30° \le \theta < 60° \\ 0.6 - \dfrac{0.6}{15}(\theta - 60°), & 60° \le \theta < 75° \\ 0, & 75° \le \theta < 90° \end{cases} \qquad \text{Eq. (2.7)}$$

The piecewise function in equation 2.7 is plotted in Figure 2.3, and a familiar pattern for IAM is observed.

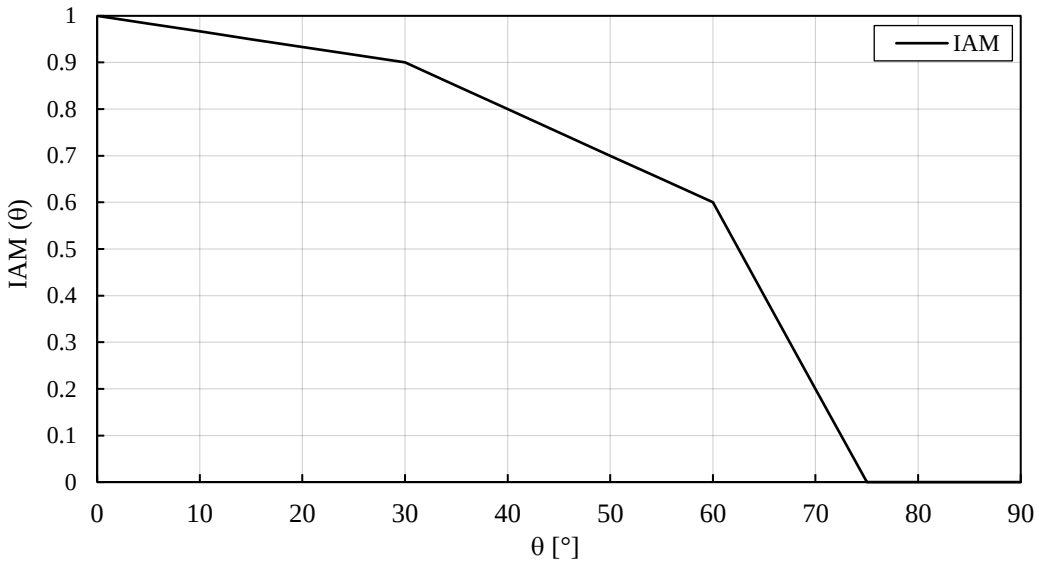

Figure 2.3. IAM function used in the model that captures generic IAM characteristics for PowerTrough 110

2.2.1.2 Calculation of Heat Transfer to Environment

Due to the temperature difference between the HTF and the ambient air, some of the absorbed heat is transferred to the environment. For heat transfer estimation, solely a limited number of data points are presented with a line fit in the manufacturer's datasheet [79]. The data points cover only around one-third of the $(T_{avg} - T_{amb})$ temperature difference range on the lower end. The first-order line is unable to

capture the fourth-order radiative heat transfer characteristics in the remaining two-thirds of the range. Therefore, extrapolating the line gives a misleading maximum attainable temperature for PowerTrough 110.

Using the experimental data provided by the manufacturer and the fact that the maximum operating temperature of the collector being 130°C, a new fourth-order fit is employed in the heat transfer calculations of the present study. Ambient temperature is assumed to be 20°C in the curve-fit procedure. The driven fourth-order heat transfer to ambient correlation is as follows:

$$\dot{Q}'_{ht-amb,col} = c_0 + c_1\left(T_{avg} - T_{amb}\right) + c_4\left(T_{avg}^4 - T_{amb}^4\right) \qquad \text{Eq. (2.8)}$$

where care must be taken in units when using equation 2.8. In equation 2.8, $\dot{Q}'_{ht-amb,col}$ is in W m^{-1}, and the coefficients c_0, c_1, and c_4 have values 0 W m^{-1}, 7.051x10^{-2} W m^{-1} K^{-1} and 3.084x10^{-8} W m^{-1} K^{-4}, respectively. Using equation 2.8 for heat transfer to ambient estimation leads to collector efficiency versus reduced temperature difference in Figure 2.4.

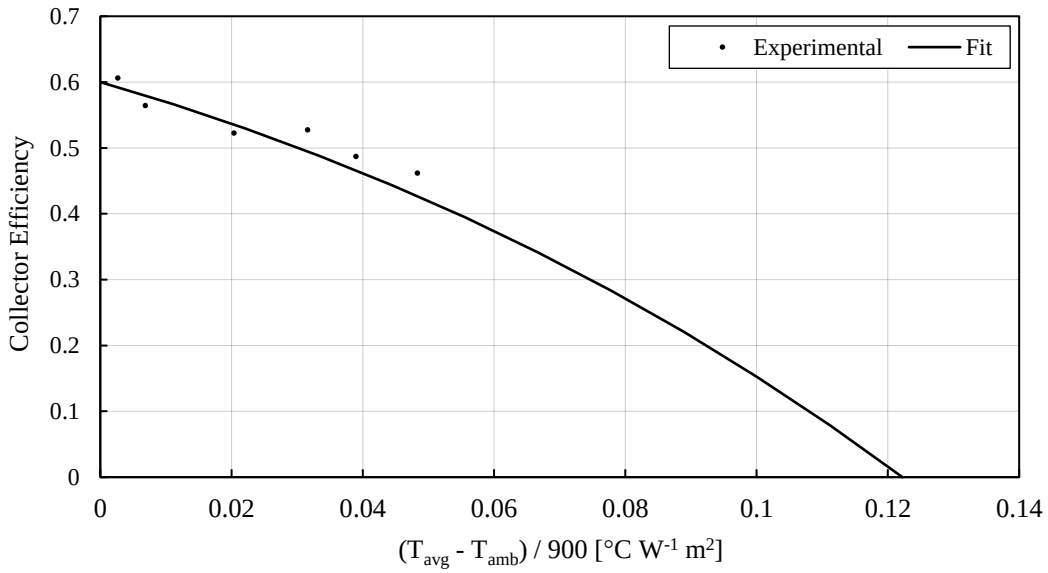

Figure 2.4. Collector efficiency snapshots of PowerTrough 110. Based on equation 2.8 and experimental data provided in the datasheet [79]

2.2.1.3 Finite Volume Method Solution to the PTC Model

The analytical solution to Equation 2.3 becomes fairly complex due to the dependent variable, temperature, appearing both in the velocity term and on the right-hand side in the heat transfer term. Finite volume method solution is employed to obtain the unsteady temperature distribution in the PTC receiver pipe. An explicit approach is preferred to obtain a new temperature distribution as time marches forward.

The time domain is discretized using the backward Euler method; whereas, the spatial domain in the convective term is discretized using first-order upwind discretization. Equations 2.3 and 2.4 can be written in the discretized form as follows:

$$\frac{T_i^{n+1} - T_i^n}{\Delta t} + V^{n+1} \frac{T_i^{n+1} - T_{i-1}^{n+1}}{\Delta x} = \frac{\dot{Q}'_{abs}{}^{n} - \dot{Q}'_{ht-amb,col}{}_i^{n}}{\rho\, c_p\, A_c} \qquad \text{Eq. (2.9)}$$

$$V^{n+1} = \begin{cases} 0, & \dot{Q}_{abs}^n < \dot{Q}_{ht-amb,col}^n \\ V_{nom}, & \dot{Q}_{abs}^n \geq \dot{Q}_{ht-amb,col}^n \end{cases} \qquad \text{Eq. (2.10)}$$

where the subscript i refers to the i^{th} control volume and n indicates the time step. While n refers to n^{th} time step, i.e., the old time step that is already solved, n+1 refers to the new time step for which the solution is desired. The case of n being equal to zero points to the initial condition; whereas, i being equal to zero represents the boundary condition. Equations 2.9 and 2.10 lead to an N_t by N_x matrix for the evolution of temperature distribution along a series of collectors in time.

2.3 Thermal Storage Unit Model

In the TES unit, the HTF acts as a sensible heat storage medium. A mild thermal stratification may be observed in the storage unit due to the moderately low conductivity of the water. On the other hand, stratification is disturbed, and the

medium is mixed by two pumps, i.e., the solar pump and the process fluid pump. Therefore, the HTF in the TES unit is assumed to be rigorously mixed for moderate slenderness ratios. As a result, lumped approach is used in TES unit modeling. An extended control volume is selected for the modeling such that it includes the HTF circulated in the heat exchanger. Work addition by the process fluid pump is neglected. Mass and energy interactions of the extended tank control volume are illustrated in Figure 2.5.

The first law of thermodynamics for the extended tank control volume in differential form reads:

$$\frac{dE_{tank}}{dt} = \dot{m}\, N_{parallel}\, c_p\, (T_{end} - T_{tank}) - \dot{Q}_{ht-amb,tank} - \dot{Q}_{supply} \qquad \text{Eq. (2.11)}$$

where $\dot{m}$ is the mass flow rate per collector row and $N_{parallel}$ is the number of collector rows in series. As V_{tank} and the material properties are constants, the term dE_{tank}/dt in equation 2.11 can be written as:

$$\frac{dE_{tank}}{dt} = \rho\, V_{tank}\, c_p \frac{dT_{tank}}{dt} \qquad \text{Eq. (2.12)}$$

The $\dot{Q}_{ht-amb,tank}$ term in equation 2.11 is calculated using the overall heat transfer coefficient based on the tank's inner surface area as follows:

$$\dot{Q}_{ht-amb,tank} = U_{tank}\, A_{tank}\, (T_{tank} - T_{amb}) \qquad \text{Eq. (2.13)}$$

If a minimum pinch point temperature difference, ΔT_{pp}, can be maintained between the tank and the target process fluid temperature at the HEX outlet, T_{load}, the load is undertaken by the TES unit. Otherwise, an auxiliary heater is assumed to satisfy all the heat demand. Although solar preheating is also possible in this case, T_{tank} is allowed to raise at times when load cannot be fully satisfied. Imposing the condition on the term $\dot{Q}_{supply}$, it can be expressed as:

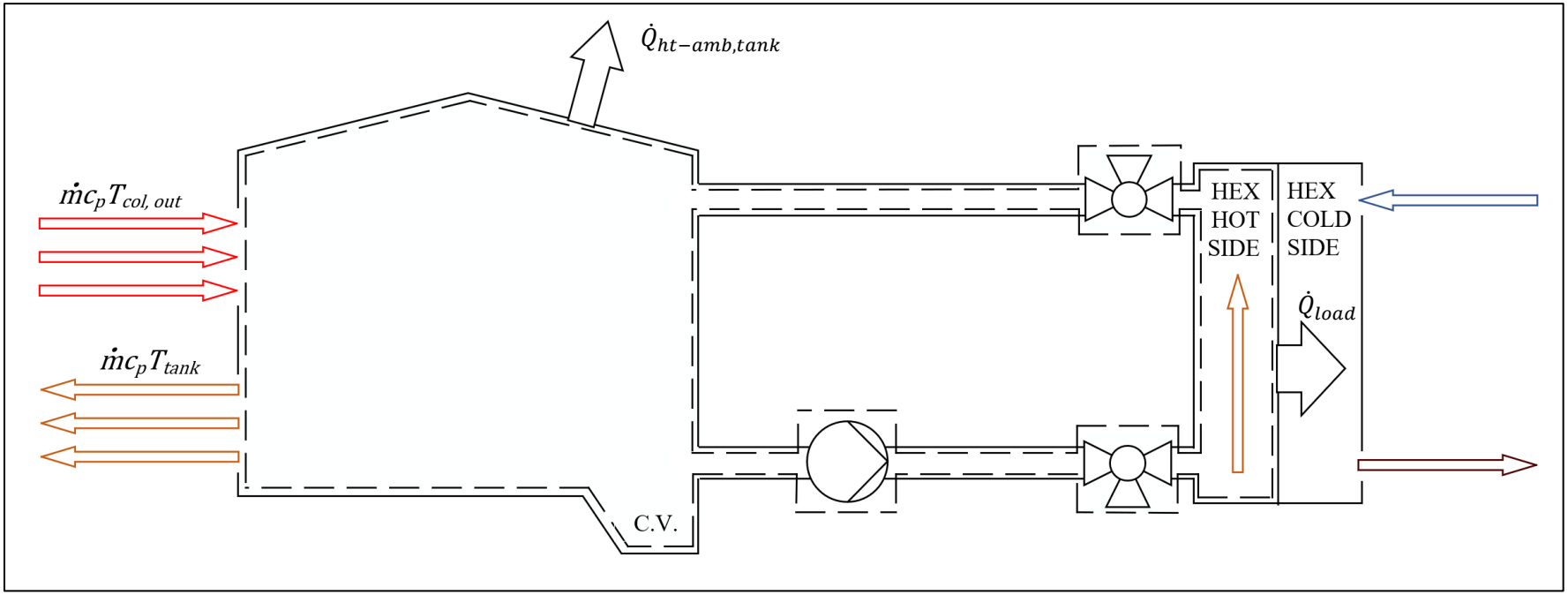

Figure 2.5. Mass and energy interactions of the extended tank control volume.

$$\dot{Q}_{supply} = \begin{cases} 0, & T_{tank} < T_{load} + \Delta T_{pp} \\ \dot{Q}_{load}, & T_{tank} \geq T_{load} + \Delta T_{pp} \end{cases} \quad \text{Eq. (2.14)}$$

Using the backward Euler method for time domain discretization, equations 2.11 and 2.13 are discretized as follows:

$$\frac{E_{tank}^{n+1} - E_{tank}^{n}}{\Delta t} = \dot{m}^{n+1} N_{parallel} c_p (T_{load}^{n+1} - T_{tank}^{n+1}) - Q_{supply}^{n+1} - Q_{ht-amb,tank}^{n} \quad \text{Eq. (2.15)}$$

$$Q_{ht-amb,tank}^{n} = U_{tank} A_{tank} (T_{tank}^{n} - T_{amb}^{n}) \quad \text{Eq. (2.16)}$$

In the numerical solution, it must further be ensured that the tank temperature does not drop below (T_{load} + ΔT_{pp}) once the load is undertaken by the TES unit, i.e., at the end of the time step. So, the term q_{supply}^{n} is discretized as:

$$Q_{supply}^{n+1} = \begin{cases} 0, & T_{tank}^{n} < T_{load}^{n+1} + \Delta T_{pp} + \dfrac{Q_{ht-amb,tank}^{n} + Q_{load}^{n+1}}{\rho V_{tank} c_p \left(1/\Delta t\right)} \\ Q_{load}^{n+1}, & T_{tank}^{n} \geq T_{load}^{n+1} + \Delta T_{pp} + \dfrac{Q_{ht-amb,tank}^{n} + Q_{load}^{n+1}}{\rho V_{tank} c_p \left(1/\Delta t\right)} \end{cases} \quad \text{Eq. (2.17)}$$

It is worth noting that the possibility of the tank being cooled by the recirculated HTF stream is eliminated in equation 2.10. The system of equations 2.15 through 2.17 leads to a column of N_t rows to be solved as time is marched forward.

2.4 The Solar Pump Model

At the exit of the TES unit, the pump is present. It is operated at constant speed; hence, modeled as a steady element. Although the solar loop piping contains numerous elements such as the mainline (large in diameter), valves, and fittings, the

load on the solar pump is primarily due to the HTF circulated in the series of small diameter receiver pipes. Therefore, only the power required to pump HTF in the collector field is considered in the present case. Pumping power is calculated by the relation:

$$W_{pump} = \frac{1}{\eta_{pump}} \frac{N_{parallel}\, \dot{m}}{\rho}\, \Delta P \qquad \text{Eq. (2.18)}$$

where the pressure drop in a series of receiver pipes, ΔP, is given as:

$$\Delta P = \frac{8}{\pi^2} \frac{N_{series}\, L_{col}\, f}{\rho\, D_{i,rec}^5}\, \dot{m}^2 \qquad \text{Eq. (2.19)}$$

The friction factor, f, in equation 2.19 is solved iteratively by the Colebrook equation [82]. The first law of thermodynamics for solar pump reads:

$$W_{pump} = N_{parallel}\, \dot{m}\, c_p\, (T_0 - T_{tank}) \qquad \text{Eq. (2.20)}$$

The pump model is connected to the complete plant simulation as follows:

$$T_0^{n+1} = \begin{cases} T_{tank}^n + \dfrac{W_{pump}^{n+1}}{N_{parallel}\, \dot{m}^{n+1}\, c_p}, & \dot{m}^{n+1} = \dot{m}_{nom} \\ N/A, & \dot{m}^{n+1} = 0 \end{cases} \qquad \text{Eq. (2.21)}$$

As the temperature distribution in the PTC receiver pipe and the tank temperature are solved for n^{th} time step, the solution for $(n+1)^{th}$ time step starts with evaluating equation 2.21 to set the inlet boundary condition of the PTC receiver pipe.

CHAPTER 3

SHIP PLANT SIMULATION – NOMINAL CASE

In the previous chapter, the suggested uncontrolled plant is described, and the sub-models of components are developed and discretized for numerical solution. In this chapter, the developed tool to simulate the constant-speed-pump-integrated SHIP plant is described, nominal case inputs are methodologically determined, and the simulation results for the nominal case are presented.

3.1 Inputs to The Simulation Tool

The developed tool takes the inputs presented in Table 3.1, filled with nominal case inputs in advance. In the upcoming titles, the procedure followed to determine the nominal case inputs is explained.

Table 3.1 Nominal Case Independent Inputs (*: Independent Inputs)

Symbol	Value	Unit	Description
Collector Properties			
*W_{col}	1.100	m	Concentrator Aperture Width
*L_{col}	3.060	m	Collector Length
A_{ap}	3.366	m^2	Aperture Area of Concentrator
*$D_{i,\,rec}$	25.40	mm	Inner Diameter of Receiver Tube
$\eta_{opt,\,0°}$	0.600	-	Collector Efficiency at 0° incidence angle

Table 3.1 Continued – Nominal Case Independent Inputs

Symbol	Value	Unit	Description
Collector Field			
$*N_{series}$	5	-	Number of Collectors in Series in One Row
$N_{parallel}$	40	-	Number of Collector Rows in Parallel
$*N_{col}$	200	-	Total Number of Collectors
$A_{ap,\ tot}$	673.2	m^2	Total Aperture Area of Collector Field
TES Unit – HTF Storage Tank			
$*(H/D)_{tank}$	1.000	-	Storage Tank Slenderness Ratio
$*V_{tank}$	13.51	m^3	Storage Tank Volume
H_{tank}	2.582	m	Inner Height of Storage Tank
D_{tank}	2.582	m	Inner Diameter of Storage Tank
A_{tank}	31.41	m^2	Storage Tank Inner Surface Area
$*U_{tank}$	2.250	$W\ m^{-2}\ K^{-1}$	Storage Tank Overall Heat Transfer Coefficient Based on Inner Surface Area
HTF Properties at 90°C Mean Temperature			
$*\rho$	965.3	$kg\ m^{-3}$	Density
$*c_p$	4206	$J\ kg^{-1}\ K^{-1}$	Specific Heat at Constant Pressure
$*\mu$	$3.150x10^{-4}$	Pa sec	Dynamic Viscosity
ν	$3.263x10^{-7}$	$m^2\ s^{-1}$	Kinematic Viscosity
Simulation Parameters			
$*t_{start}$	19-07-2006 00:00	dd-mm-yyyy hh:mm	Starting Date and Time of Simulation
$*\Delta t$	15.00	s	Finite Time Step
$*N_t$	46080	-	Number of Time Steps
t_{end}	27-07-2006 00:00	dd-mm-yyyy hh:mm	End Date and Time of Simulation
$*\Delta x$	3.060	m	Finite Spatial Step
$*N_x$	5.000	-	Number of Spatial Steps

Table 3.1 Continued – Nominal Case Independent Inputs

Symbol	Value	Unit	Description
L_{sr}	15.30	m	Length of a Series of Collectors
CFL	0.900	-	Courant Number
$*T^0$	40.00	°C	Initial Condition
$*\Delta T_{pp}$	5.000	°C	Minimum Pinch Point Temp. Difference
$*\eta_{pump}$	0.9	-	Pump Efficiency
Flow Parameters			
$*\dot{m}_{nom}$	0.090	kg s^{-1}	Mass Flow Rate in a Series of Collectors
$\dot{m}''_{nom}$	0.018	kg s^{-1} cm^{-2}	Mass Flux in Receiver Pipes
V	0.180	m s^{-1}	HTF Flow Velocity in Receiver Pipes
Re_D	14322	-	Reynold's Number of HTF Flow in Receiver Pipes
$*\varepsilon$	1.500	mm	Receiver Pipe Surface Roughness
$\varepsilon/D_{i,rec}$	0.059	-	Receiver Pipe Relative Roughness
f_D	0.079	-	Darcy's Friction Factor

3.2 Determining the Nominal Case Inputs

The collector properties in Table 3.1 have been specified once the collector is selected. The procedure is continued by determining the independent inputs $(H/D)_{tank}$, U_{tank}, η_{pump}, ε and ΔT_{pp}. Both extremes of the storage tank slenderness ratio result in a large surface area for a given volume that would increase heat transfer from the tank. Also, a very slender tank diminishes the lumped model's validity. Despite the mixing effect of two pumps connected to the storage unit, a large α/H^2 coefficient ($Fo = \alpha t/H^2$) and a small Biot number ($Bi_D = UD/k$) are desirable for holding the lumped assumption. Stratified TES model's (H/D) ratios in literature are taken as 2 [44,67]. Taking all these statements into account, the slenderness ratio of

the storage tank is selected to be 1. The overall heat transfer coefficient of the insulated storage tank is set to 2.25 W m^{-2} K^{-1} [83]. The value of 0.9 is entered for the solar pump efficiency at the pump's operating point. Tubing surface roughness is taken as 0.0015 meters. For ΔT_{pp}, small values lead to ineffective use of heat exchanger length; whereas, large values result in less heat load to be satisfied by solar heat. ΔT_{pp} is set to 5°C; that is, the bottom end of the recommendation in [10]. The initial condition T^0 is selected as 40°C so that quick start-up of high-capacity TES is ensured while avoiding unfair advantage to high-capacity systems.

The optimum values for the yet unspecified inputs vary on the dynamic operating conditions of the SHIP plant. Therefore, it is useful to determine the remaining input values with respect to a fixed design point. The design point is given in Table 3.2 is assumed to be operated at the DNI available hours. Direct Normal Irradiation (DNI) available hours in Table 3.2 are specified such that they best match with Graz's DNI pattern in the summer season on a clear day.

Table 3.2 Nominal Case Design Point

Symbol	Value	Unit	Description
DNI	900	W m^{-1}	Direct Normal Irradiation
-	08:30 – 16:30	hh:mm	DNI Available Hours (Local Time)
θ	0	°	Solar Incidence Angle
T_{amb}	20.0	°C	Ambient Temperature
$(T_{avg,col} - T_{tank})$	5.00	°C	The Difference between Average Temperature in the Collector Field and the HTF Temperature in TES Unit

The parameters N_{col} and V_{tank} collectively impact the overall system performance; so, they are taken into consideration as a pair. It is desirable to obtain reasonable values for them; as, the values emphasize a reference point for further exploration of the input domain in the parametric analysis part. For this purpose, an auxiliary, computationally lightweight, 0D transient SHIP plant model is developed in MS

Excel. Then, a multi-input optimization for (N_{col}, V_{tank}) pair is conducted on the 0D transient model. While the input values $(H/D)_{tank}$, U_{tank}, ΔT_{pp} and T^0 determined for the actual simulation are used unchanged in the 0D-transient model, the pumping power is neglected. The auxiliary model calculates the heat transfer from the collectors based on $T_{avg,col}$, and takes the transfer from the storage tank into account. The condition in equation 2.17 is embedded into 0D model's T_{tank} calculation, as well. 12-day simulations are run using time step of 3 minutes to ensure that the system is reached to steady-periodic state, even for large V_{tank} values. The KPIs of solar fraction, f_{solar}, and useful heat supplied to the load by each collector per day, $Q_{supply,\ avg,\ col}$, are evaluated at the end of simulations. The definition for the KPIs are given in more detail in section 3.5.

When $Q_{supply,\ avg,\ col}$ is asked to be maximized for the actual load profile, the solver sets the (N_{col}, V_{tank}) tuple to the value of (25.60, 23.52 m^3), corresponding to f_{solar} of 11.03% and $Q_{supply,\ avg,\ col}$ of 10.74 kWh day^{-1} col^{-1}. The point where the solution converges suggests satisfying almost all of the 40°C portion of the load, that is 11.76% of the complete load profile by duration. The point where V_{tank} converges implies that most of the 40°C portion is aimed to be satisfied to maximize $Q_{supply,\ avg,\ col}$. The case of aiming for the 40°C part of the load could have been achieved using FPC technolgy and renders the present analysis unreasonable. A greater f_{solar} is expected from the PTC-integrated SHIP plant. To force the solver to converge to a point of greater f_{solar}, the temperature of the 40°C part in the load profile is replaced with 74°C, keeping the heat load constant. Re-run of the optimization resulted in the tuple value of (192.6, 13.51 m^3). The result of the second run gives f_{solar} of 63.09% and $Q_{supply,\ avg,\ col}$ of 8.165 kWh day^{-1} col^{-1} for the modified load profile; whereas, for the original load profile gives f_{solar} of 63.68% and $Q_{supply,\ avg,\ col}$ of 8.241 kWh day^{-1} col^{-1}. Time series T_{tank}, modified (T_{load} + ΔT_{pp}) and Q_{exess}; that is, the excess thermal energy stored are presented in Figure 3.1. Q_{excess} at the end of the simulation should be small compared to heat load and absorbed heat. The difference between Q_{excess} at the beginning and at the end of the day being small indicates that the stored fraction of absorbed solar heat is minimal. Although the

simulation period is 12 days, only four days are shown in Figure 3.1; since, the system reaches to steady periodic state in 2 days. The period in which the load demand is completely supplied by solar heat is observable; that is, when T_{tank} is above (T_{load} + ΔT_{pp}). At intervals where T_{tank} and (T_{load} + ΔT_{pp}) overlap, it could be said that heat load is partially satisfied by solar heat. Figure 3.1 uncovers that the system partially aims for both 85°C and 74°C parts of the heat load. Having obtained an f_{solar} value that makes installing PTCs to the site justifiable, the load profile is not further modified. V_{tank} is set to 13.51 m^3, while N_{col} is set to the integer value of 200. The impact of load profile, V_{tank} and N_{col} is discussed in detail in section 4.1.

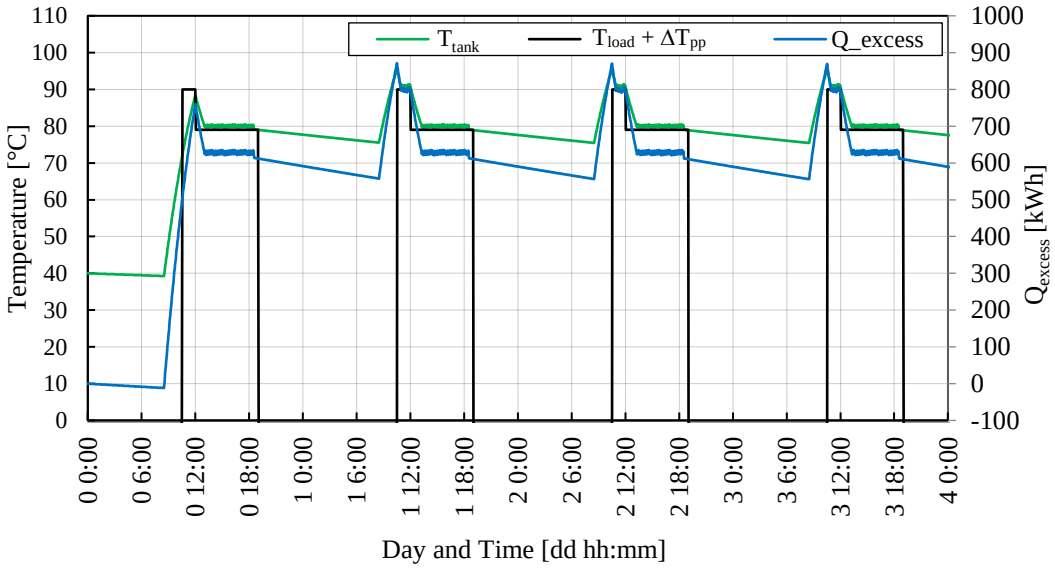

Figure 3.1. Auxiliary 0D transient simulation results for optimized N_{col} and V_{tank} on modified load profile.

In Figure 3.1 T_{tank} fluctuates approxiamately between 75 and 95°C. And the parameter ($T_{avg,col}$ - T_{tank}) suggests that $T_{avg, col}$ oscillates between 80 and 100°C. So, HTF properties at 90°C are used in the nominal case input set. The procedure is continued with determining the mass flow rate in a series of collectors.

The mass flow rate that sets the Reynold's number ($Re_D = VD/\nu$) in fully turbulent regime, greater than 4000, is desirable for enhanced heat transfer. On the other hand, it should be small enough to circulate the HTF in the collector field with reasonable pumping power. The nominal mass flow rate, $\dot{m}_{nom}$, is determined as 0.09 kg/s, corresponding to the Reynolds number of ~14300 at 90°C. The selection ends up on the safe side as viscosity is sensitive to changes in temperature. Smaller values for Reynold's number are observable when HTF is colder than 90°C. It is also worth noting that Pe number becomes ~28600 as a result of the flow rate selection. So, the validity of neglecting axial conduction is ensured. As the nominal mass flow rate is fixed, the parameters of collector field configuration, N_{series} and $N_{parallel}$, can be determined accordingly.

The temperature difference, ($T_{avg,col}$ - T_{tank}), being determined as 5°C at the design point implies the temperature to be increased by approximately 10°C from inlet to exit through a series of collectors. An inlet temperature of 90°C is considered; so, the heat transfer from collectors to ambient takes place at an average temperature of 95°C. N_{series} that renders T_{end} as 100°C for 0.09 kg/s flow rate is calculated as 4.91 and ceiled to 5. As a result, $N_{parallel}$ is set to 40.

Having determined all physical parameters, the procedure is continued with simulation parameters. Spatial time step, Δx, is selected as being equal to the collector length, 3.06 meters. The upper limit for the time step, dt, is dictated by the Courant Friedrichs Lewy (CFL) number ($CFL = V\,dt/dx$) of unity. With the selected $\dot{m}_{nom}$ and Δx, dt is entered the value of 15 seconds that sets CFL to 0.9.

The simulation is run for 46080 time steps; that corresponds to 8 days. The duration of 8-days allows proper performance comparison of systems if V_{tank} is less than $20m^3$; because, the duration is selected as being equal to several multiples of start-up times. On the other hand, the number of time steps give reasonable execution time and memory allocation on an average personal computer. As both sunny and cloudy hours are encountered throughout, the interval between 19-07-2006 00:00 and 27-07-2006 00:00 is selected as the simulation period.

3.3 Solar Radiation and Meteorological Data

The solar radiation data is obtained from Helioclim-3 archives version hc3v5 in 15-minute intervals. The meteorological data provided by Modern Era Retrospective Analysis for Research and Applications – 2 (MERRA-2) satellite is employed [84]. The data are extracted for the location of Graz (lat: 47.071, lon: 15.438) for the relevant interval is given along with nominal case results in section 3.6. As the simulation period is set to eight days, there is no point in using Typical Meteorological Year (TMY) data. However, if more computational power is available, it is recommended to simulate the entire season with TMY data for the target location.

3.4 Program Flow

The simulation is coded in VBA language. Meteorological data and the load profile are supplied to the program as comma-separated values. The code can search and read the relevant data from datasets, which is useful when working with large datasets. Simulating multiple cases, writing the outputs to a target file, automatized post-processing are implemented features. A modular architecture is employed for ease of modification and further development of the code. Although VBA is an object-oriented language, procedural programming paradigm is followed in the main structure of the program. The program flow chart for the simulation of a single case is illustrated in Figure 3.2. To simulate multiple cases, the routine in Figure 3.2 is automatically executed a certain number of times.

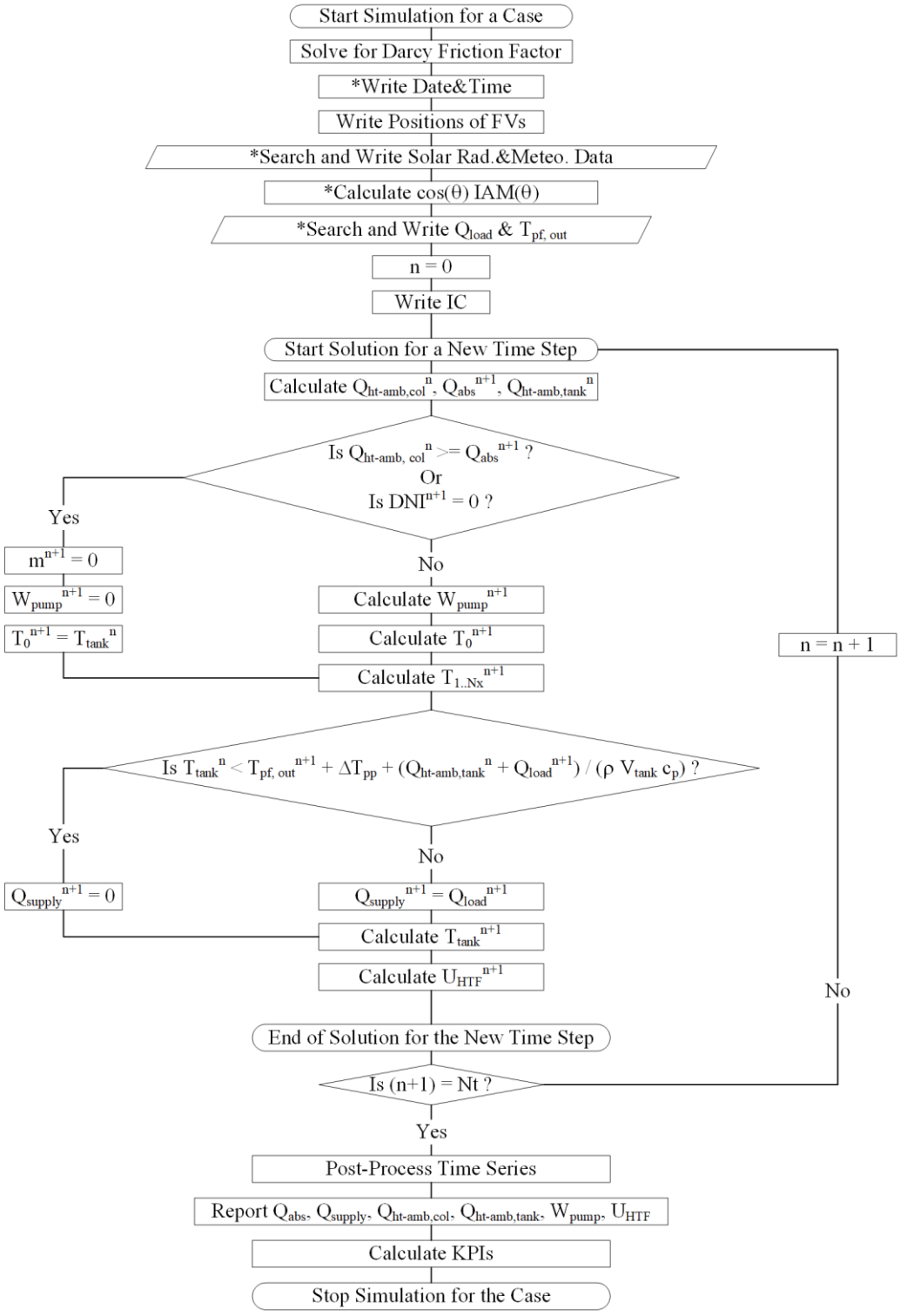

Figure 3.2. The program flow chart (*: Do for all time steps)

3.5 Outputs of the Simulation Tool

The simulation tool takes the previously given inputs, processes them according to the procedure given in the program flow chart, and produces outputs in a matrix. The output matrix has N_t + 1 rows and for each time step outputs of temperature distribution in collectors, T_{tank}, W_{pump}, Q_{abs}, $Q_{ht\text{-}amb}$ and Q_{supply} are reported in columns. The output matrix consists of bulk numbers and usually end up being fairly large. To help the user draw insightful conclusions from the output matrix, the most remarkable time series are plotted automatically. In addition, some abstract values, namely KPIs, that indicate the overall plant performance are extracted from the output matrix. In the following paragraphs, the KPIs are introduced.

The main objective of the SHIP plant is to reduce the need for the fossil-fuel-based auxiliary heater. The solar fraction, f_{solar}, indicating what fraction of the total heat load is undertaken by solar heat is defined as follows:

$$f_{solar} = \frac{Q_{supply}}{Q_{load}} \qquad \text{Eq. (3.1)}$$

The system gains energy by the absorbed solar irradiation and by the pump electrical work input, $(Q_{abs} + W_{pump})$. The total energy gain by the term $(Q_{abs} + W_{pump})$ is either lost to the environment from the collectors, $Q_{ht-amb,col}$, and from the storage tank, $Q_{ht-amb,tank}$, or supplied to the process, Q_{supply}. And the remaining thermal energy, $(U_{HTF,final} - U_{HTF,ref})$, is stored in the HTF. Also, as the finite volume method is used, a numerical residual error is expected in the energy balance. Including the numerical residual error as a term, E_{res}, the energy balance equation for the entire SHIP plant can be written as:

$$W_{pump} + Q_{abs} - \left(Q_{supply} + Q_{ht-amb,total}\right) = U_{HTF,final} - U_{HTF,ref} - E_{res} \qquad \text{Eq. (3.2)}$$

where $Q_{ht-amb,total}$ is the sum:

$$Q_{ht-amb,total} = Q_{ht-amb,col} + Q_{ht-amb,tank} \quad \text{Eq. (3.3)}$$

It is helpful to normalize the terms in Equations 3.1 and 3.2 by $(Q_{abs} + W_{pump})$ as follows:

$$f_{abs} = \frac{Q_{abs}}{Q_{abs} + W_{pump}} \quad \text{Eq. (3.4)}$$

$$f_{pump} = \frac{W_{pump}}{Q_{abs} + W_{pump}} \quad \text{Eq. (3.5)}$$

$$f_{supply} = \frac{Q_{supply}}{Q_{abs} + W_{pump}} \quad \text{Eq. (3.6)}$$

$$f_{ht-amb,col} = \frac{Q_{ht-amb,col}}{Q_{abs} + W_{pump}} \quad \text{Eq. (3.7)}$$

$$f_{ht-amb,tank} = \frac{Q_{ht-amb,tank}}{Q_{abs} + W_{pump}} \quad \text{Eq. (3.8)}$$

$$f_{ht-amb,total} = \frac{Q_{ht-amb,total}}{Q_{abs} + W_{pump}} \quad \text{Eq. (3.9)}$$

$$f_{stored} = \frac{U_{HTF,final} - U_{HTF,ref}}{Q_{abs} + W_{pump}} \quad \text{Eq. (3.10)}$$

$$f_{res} = \frac{E_{res}}{Q_{abs} + W_{pump}} \quad \text{Eq. (3.11)}$$

The residual energy balance error term, f_{res}, is ensured to be smaller than 0.1% at the end of each run. The KPI, $Q_{supply,col}$, reflecting how effectively the collectors are utilized, is defined as:

$$Q_{supply,avg,col} = \frac{Q_{supply}}{N_{col}\, N_{days}} \quad \text{Eq. (3.12)}$$

3.6 Validation

To ensure the validity of the FVM solution to the 1D PTC sub-model, a simulation is run with the same input set as the reference study, and the results are compared. Specifically, the comparison is made against Noureldin et al.'s [65] and Bubolz's [64] studies. In both studies, the receiver pipe wall is included in the problem domain, and the energy balance equations for the receiver pipe wall and the HTF are coupled. Also, temperature-dependent material properties are used in [35] and [36]. Geometric and material properties are presented in [64]. Noureldin et al. compared their model to Bubolz's; in addition, to experimental data obtained from the ANDASOL-3 solar field. The results of [65] and [64] very tightly overlap on top of each other, while results of [65] follow the experimental data closely.

The input set that is used for the comparison of results is given in Table 3.3, and the results are compared in Figure 3.3. The deviation between the present study results and the compared references is marginally small. So, the results of reference [64] are not added to Figure 3.3.

Table 3.3 Validation input set

Symbol	Value	Unit	Description
Collector Properties			
W_{col}	5.450	m	Concentrator Aperture Width
$D_{i,\,rec}$	64.00	mm	Inner Diameter of Receiver Tube
$\eta_{opt,\,0°}$	0.750	-	Collector Efficiency at 0° incidence angle
HTF: Molten Salt (60% $NaNO_3$ – 40% KNO_3)			
ρ	2300	kg m^{-3}	Average Density of Domain
c_p	1690	J kg^{-1} K^{-1}	Average Specific Heat at Constant Pressure

Table 3.3 Continued – Validation input set

Symbol	Value	Unit	Description
Simulation Parameters			
Δt	1.000	sec	Finite Time Step
N_t	4500	-	Number of Time Steps
Δx	10.00	m	Finite Spatial Step
N_x	100	-	Number of Spatial Steps
L_{sr}	1000	m	Length of a Series of Collectors
CFL	0.099	-	Courant Number
T^0	290.0	°C	Initial Condition
Flow Parameters			
$\dot{m}$	7.300	kg s^{-1}	Mass Flow Rate in a Series of Collectors
V	0.987	m s^{-1}	HTF Flow Velocity in Receiver Pipes

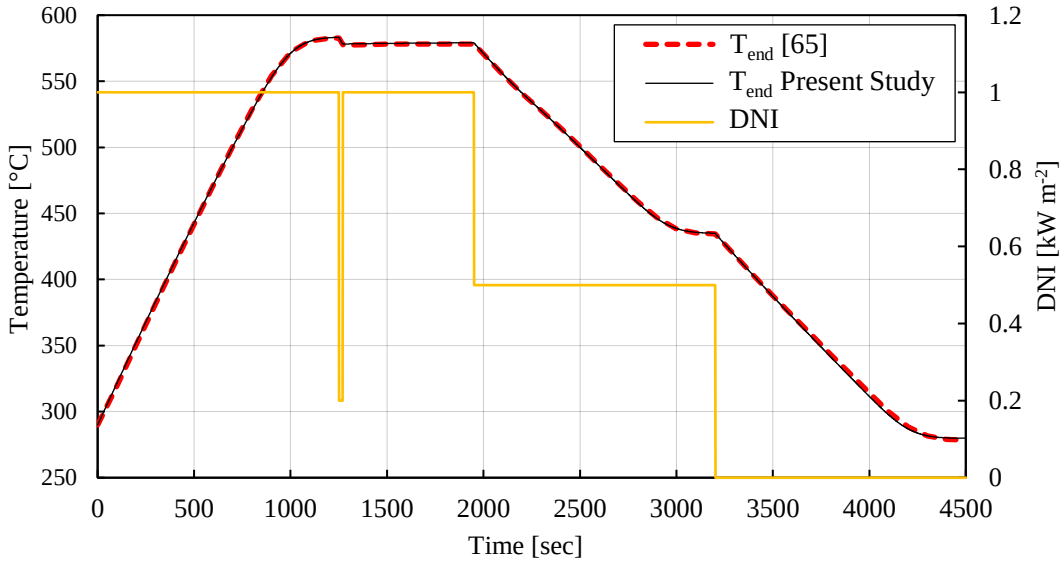

Figure 3.3. Comparison of FVM solution of PTC model results for molten salt in ANDASOL-3 solar field with reference [65]

3.7 Simulation Results of Nominal Case

The simulation is run with nominal case inputs and the time series of T_{end}, T_{tank}, (T_{load} + ΔT_{pp}) and $\dot{m}$ are presented along with meteorological data in Figure 3.4. It can be deduced from Figure 3.4 that T_{end} asymptotically approaches to T_{amb}, as expected, when the pump is stopped as a result of the condition in equation 2.10. The pump shutting off action at small or zero DNI is distinctly executed at once, without any hesitation. The shutting-off action takes place at the intersection point of series T_{end} and T_{tank}; in other words, when the HTF in the collectors is at the same temperature as the storage tank and the temperature distribution is smooth. However, the condition in equation 2.10 leads to chattering when turning the pump on. Due to the HTF being cooled down at night or at cloudy hours, a small DNI is sufficient to trigger the pump being turned on. As a result, part of the receiver pipe is immediately filled with relatively hot HTF from the tank. So, the condition is unmet, and the pump is turned off until DNI rises to a level that triggers the turning-on action again. Nevertheless, the condition ensures net energy gain to the system. Despite being chattered, pump turning on action is executed when DNI reaches to the critical value.

T_{end} rise pattern is observed to be non-linear, asymptotically approaches to steady temperature. The difference between T_{end} and T_{tank} increases with increasing DNI is as expected. It could be concluded that the heat load is completely satisfied using solar heat when T_{tank} is greater than (T_{load} + ΔT_{pp}), and partially satisfied when T_{tank} and (T_{load} + ΔT_{pp}) overlap on top of each other. The series T_{end} and T_{tank} experience sharp changes at the points where the load is applied or released from the solar system. This is because the load of 292.2 kW is instantly applied neglecting any thermal inertia. As a result, the rate of change of T_{tank} suddenly becomes negative. Following T_{tank}, the collectors are completely filled with the HTF at the T_{tank} temperature within a few time steps and a similar sharp change is observed also in the series T_{end}. In reality; however, T_{tank} and T_{end} functions are expected to be smooth, since the load cannot be introduced suddenly. Thermal inertia of the heat exchanger,

piping, HTF being zero, prevent sharp changes in rate of change of temperature values.

A dip in the mid-day for the DNI cos(θ) IAM(θ) term is observed as the solar incidence angle is smaller in mid-day. A larger gap is expected between DNI and DNI cos(θ) IAM(θ) series in the winter time. In fact, the series T_{end} and T_{tank} fluctuate as DNI suddenly changes and pump is suddenly turned on and off. The amplitude of fluctuations is very small since the tank volume is 43.6 multiple of the volume of HTF in the collector side. The PTC model neglecting axial conduction effects results in fluctuations to last longer.

The KPIs f_{solar} and f_{supply} are re-calculated for daily periods and change of KPIs during the simulation periods is presented in Figure 3.5. In addition, daily Q_{abs} values are presented in Figure 3.5. For the KPIs f_{solar} and f_{supply}, weighted-averages i.e. the original output of simulation tool is included in the figure; whereas, for Q_{abs} average is included at the "AVG" column.

Final cumulative terms in equation 3.2 and KPIs of nominal case simulation are given in Table 3.4.

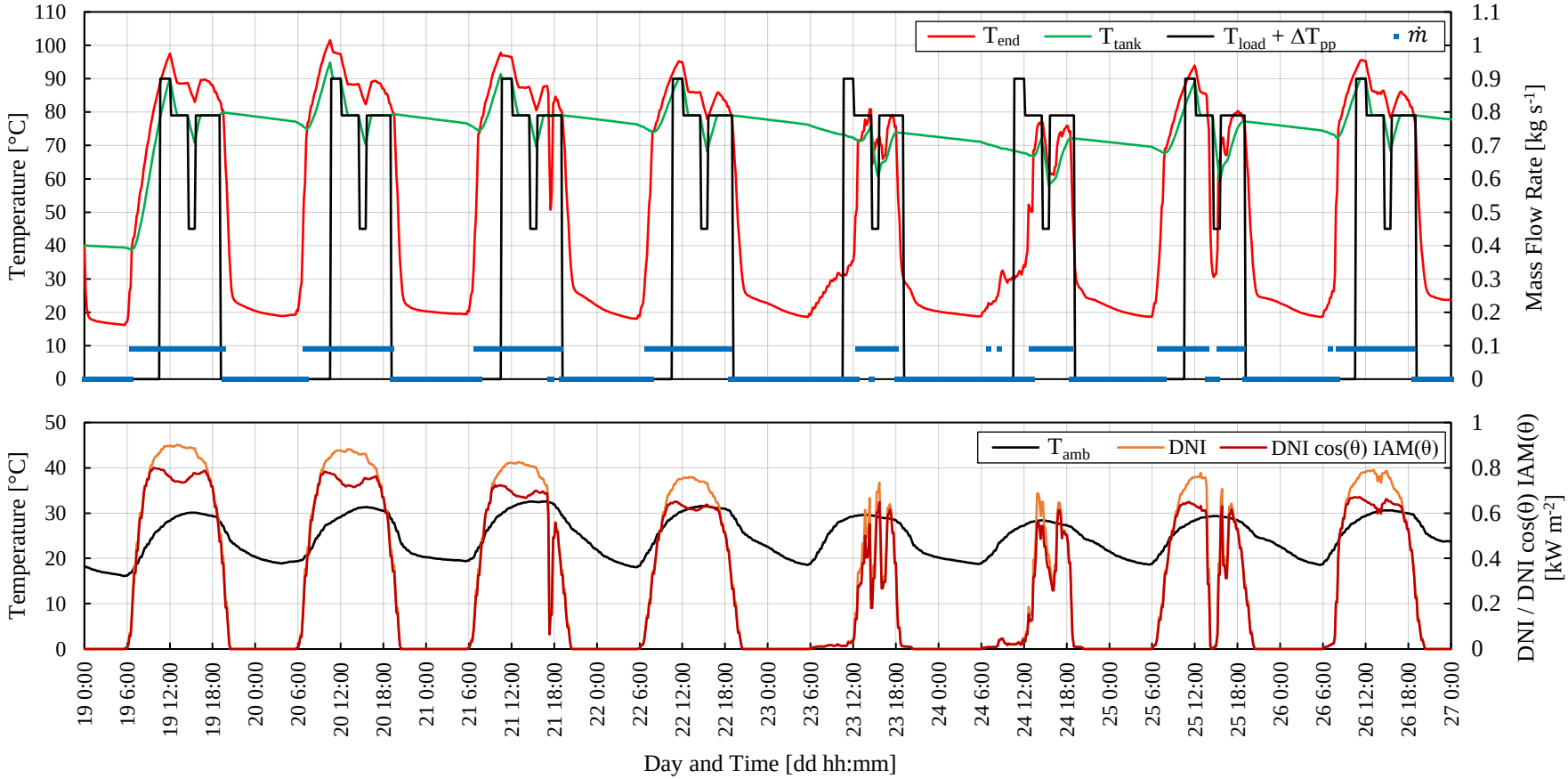

Figure 3.4. Nominal case simulation results of series T_{end}, T_{tank}, m, and the meteorological data (Horizontal gridlines are aligned).

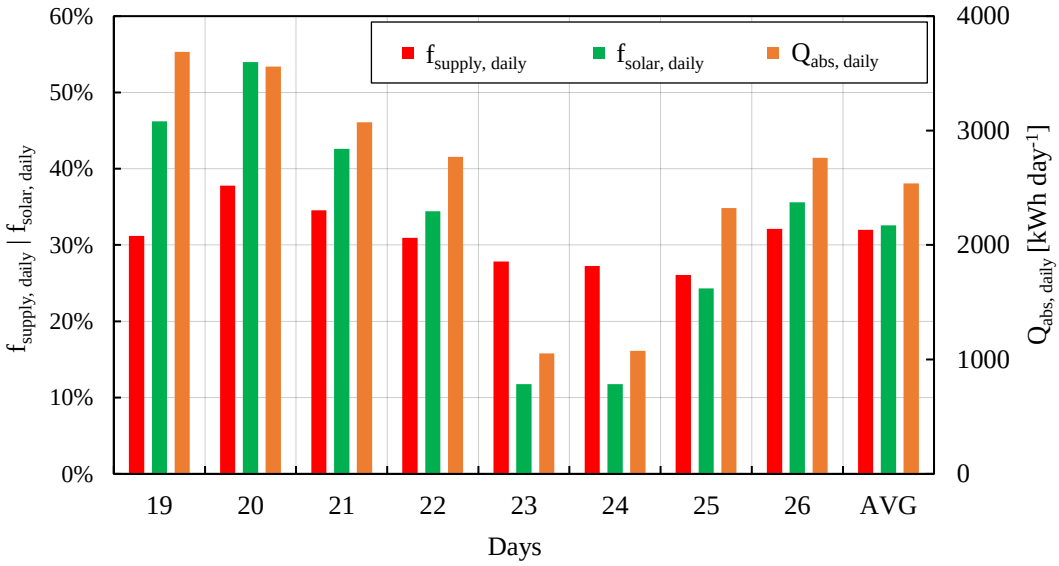

Figure 3.5. Daily calculated KPIs f_{solar}, f_{supply} and cumulative daily absorbed solar heat for the nominal case

Table 3.4 Output energy balance terms and KPIs for nominal case simulation (*:$Q_{supply,\ avg,\ col}$ in kWh day^{-1} col^{-1})

Symbol	Value [kWh]	Symbol	Value
Q_{abs}	20306	f_{abs}	99.95%
W_{pump}	10.099	f_{pump}	0.05%
Q_{load}	19939	f_{solar}	32.58%
Q_{supply}	6496.1	f_{supply}	31.97%
$Q_{ht-amb,col}$	12570	$f_{ht-amb,col}$	61.87%
$Q_{ht-amb,tank}$	675.12	$f_{ht-amb,tank}$	3.32%
$Q_{ht-amb,total}$	13245	$f_{ht-amb,total}$	65.19%
$U_{HTF,final} - U_{HTF,ref}$	569.95	f_{stored}	2.81%
E_{res}	5.2777	f_{res}	0.03%
$Q_{supply,avg,col}$	*4.0601		

It can be deduced from Figure 3.5 that; although, Q_{abs} decreases slightly from day 19^{th} to 20^{th} $f_{solar,\ daily}$ and $f_{supply,\ daily}$ increases, because a significant amount of Q_{abs} is used to warm up the storage tank. The KPI $f_{supply,\ daily}$ is observed to be relatively small in cloudy days compared to sunny days. Figure 3.5 also gives the chance of comparing the results against the auxiliary 0D model. For the day 20^{th} f_{solar} of 0.54 is obtained for $Q_{abs,\ daily}$ of 3558 kWh; whereas, the 0D model overestimates f_{solar} to be 0.66 and calculates $Q_{abs,\ daily}$ to be 3635 kWh with the same inputs. When DNI of 0D model is adjusted such that, it also has the $Q_{abs,\ daily}$ value of 3558 kWh, the f_{solar} prediction is updated to 0.63. Although there are many differences between the two models, the deviation mainly stems from the difference between dimensional complexity of two models. The 0D model's estimation of heat transfer to environment deviate significantly compared to 1D model's. As a result, the 0D model overestimates the collector outlet temperature for large inlet temperatures; whereas, it underestimates the collector outlet temperature for small inlet temperatures.

In table 3.4, f_{pump} is expectedly very small compared to f_{abs} for the nominal case mass flow rate. Likewise, f_{res} is found out to be small; 0.03%. Heat transfer to environment fractions indicate that the heat is mostly lost from the collector side, with the nominal case number of collectors.

3.8 Mesh Independence

In order to demonstrate the mesh independence of the FVM solution to the 1D PTC sub-model, solely a series of PTCs are simulated with the inputs in Table 3.5. Temperature distributions obtained using successively finer meshes are presented in Figure 3.6. From Figure 3.6, it can be concluded that mesh independence is achieved for the PTC FVM solution. Furthermore, the mesh used in the nominal case simulation can be regarded as a reasonably fine mesh. Figure 3.6 also verifies the previously mentioned statement that the 0D model underestimates the collector outlet temperature for small inlet temperatures.

Table 3.5 Input set for illustration of mesh independence of 1D PTC Model

Symbol	Value	Unit	Description
DNI	900	W m^{-2}	Direct Normal Irradiation
θ	0	°	Solar incidence angle
N_{series}	16	-	
T_0	40	°C	
Δt	4	sec	Differential time step
Nt	120	-	

Mesh	Symbol	Value	Unit	Mesh	Symbol	Value	Unit
Extremely Coarse (0D-Transient Model)	Δx	48.96	m	Coarse	Δx	12.24	m
	Nx	1	-		Nx	4	-
	CFL	0.015	-		CFL	0.060	-
Moderate	Δx	3.060	m	Fine	Δx	0.765	m
	Nx	16	-		Nx	64	-
	CFL	0.241	-		CFL	0.962	-

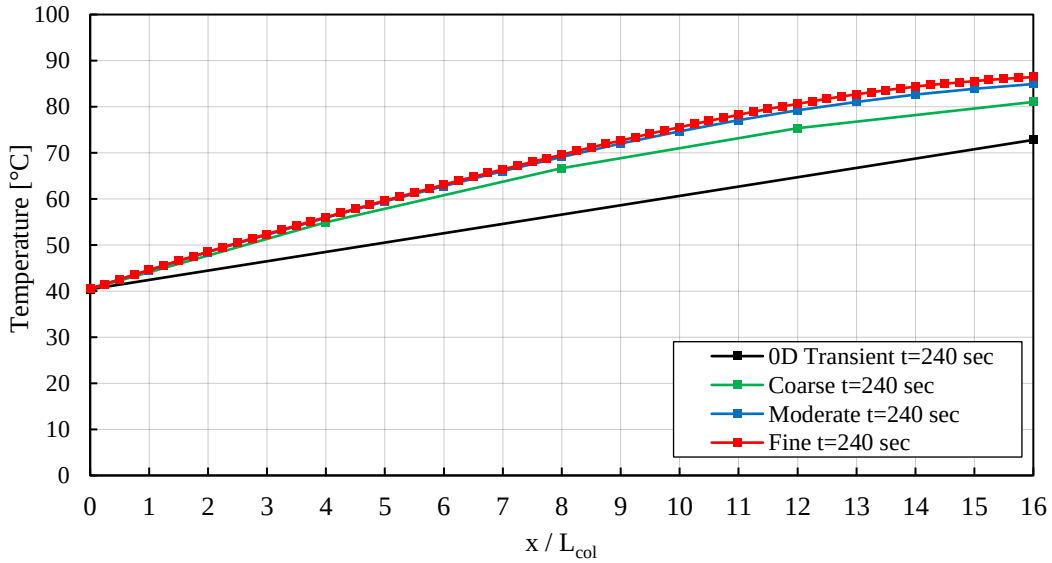

Figure 3.6. Temperature distribution in a series of PTC receiver pipes for successively varied mesh size. 0D transient model corresponds to the extremely coarse mesh.

CHAPTER 4

SHIP PLANT SIMULATION – PARAMETRIC STUDY

In the previous chapter, the simulation tool is introduced and used to obtain results for the nominal case. In this chapter, the tool is utilized for parametric analysis. Specifically, impacts of the parameters V_{tank}, N_{col}, N_{series}, $N_{parallel}$ and $\dot{m}_{nom}$ on the KPIs are investigated. Unless otherwise is specified, the analyses are conducted by varying only the parameter under investigation in the nominal case input set and holding all other inputs constant.

4.1 Impact of Parameters Storage Tank Volume and Number of Collectors

The parameters V_{tank} and N_{col} are investigated together, as it is done previously. 306 simulations are run, using a 34x9 grid in which the parameters are successively varied. The parameter N_{col} is varied by changing $N_{parallel}$ and holding N_{series} constant as it is in the nominal case input set. The results for the KPIs, $Q_{supply,avg,col}$ and f_{solar} are presented in Figures 4.1 and 4.2, respectively. In both figures local maximum on consant N_{col} lines are marked with black squares. The black squares indicate the same points in both figures. In Figure 4.1 the global maximum is observed at the value (10 m^3, 25) for (V_{tank}, N_{col}) pair; that is the third mark from the lower end of the N_{col} range. First two marks on curves of constant N_{col} for N_{col} smaller than 25 point out the opportunity to increase both f_{solar} and $Q_{supply,\ avg,\ col}$ by adding more collectors. The fourth mark from the lower end of the N_{col} range is a special one as its f_{solar} value reads 11.2%; that corresponds to the 40°C portion of the heat load by duration. The first four marks suggest aiming for the 40°C part of the load by increasing N_{col}. Only aiming for the 40°C part, more storage capacity is needed. As a result, the necessity of simultaneously increasing V_{tank} arises for optimum performance.

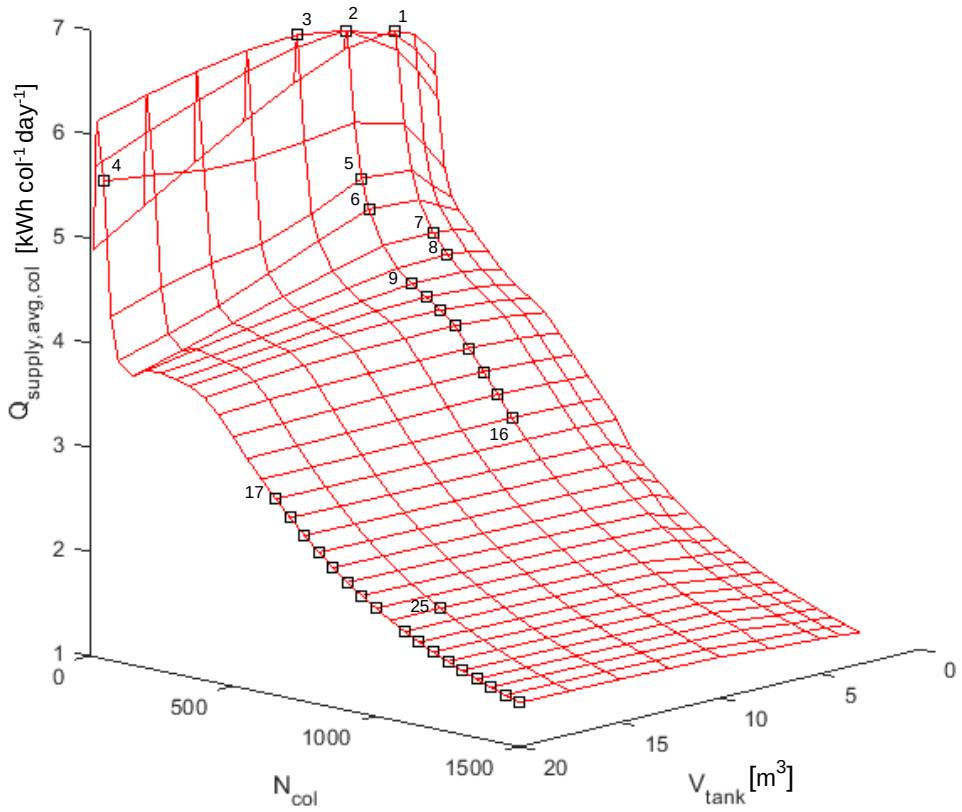

Figure 4.1. Variation of $Q_{supply,avg,col}$ as V_{tank} and $N_{parallel}$ values are varied and all other inputs are held constant at nominal case values

If the simulation were run for all sunny days, the global maximum would be observed at the point where f_{solar} is approximately equal to 11%. Due to Q_{supply} being limited in cloudy days, the effect of N_{col} in the denominator of $Q_{supply,\ avg,\ col}$ becomes dominant at an f_{solar} smaller than 11%.

Fifth mark and the following ones suggest further aiming to cover more of the 74°C parts of the load. While the optimum V_{tank} fluctuates between fast response versus more capacity, it finally saturates at the maximum value of 20 m^3 in order to keep f_{solar} increasing in such a manner that the collectors are best utilized. The actual

optimum V_{tank} values could be uncovered by enlarging the domain using more computational resources. In this case; however, simulation duration is recommended to be increased, as well.

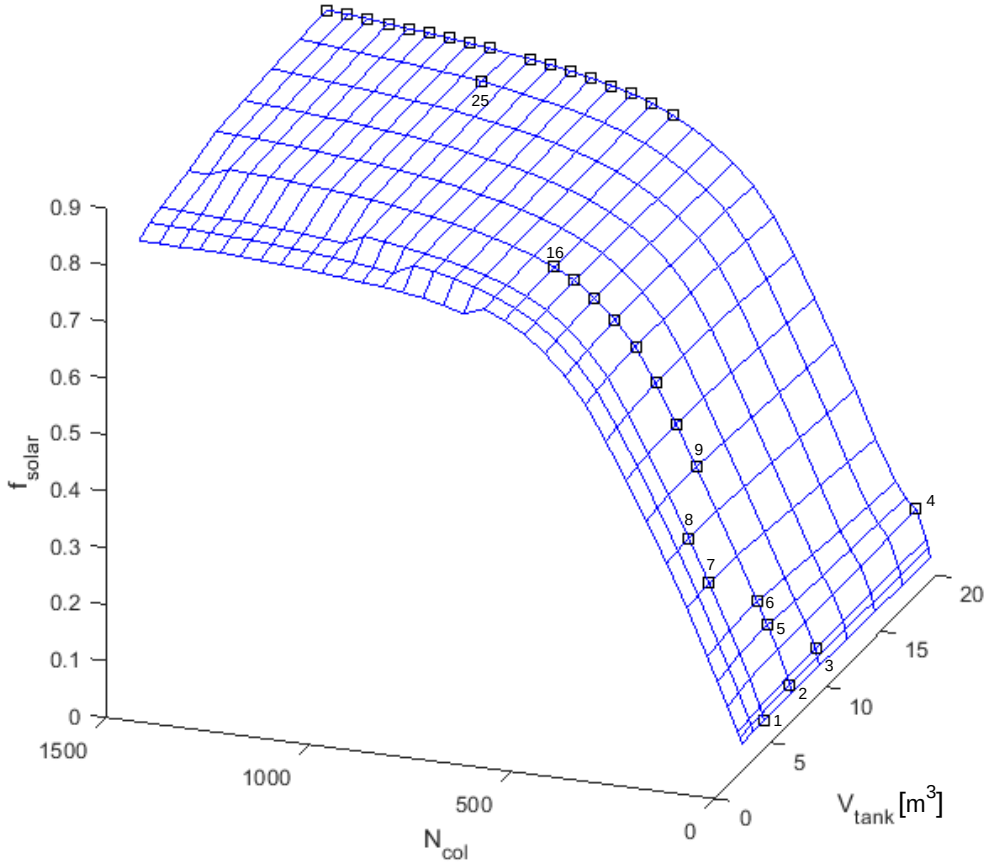

Figure 4.2. Variation of f_{solar} as V_{tank} and $N_{parallel}$ values are varied and all other inputs are held constant at the nominal case values

The optimum V_{tank} exceptionally diverges from its saturated value on the twenty-fifth mark, where f_{solar} reads 82.2%. It is attention capturing that, the portion of the heat load excluding the 85°C part is 82.4% of the total heat load by duration The twenty fifth mark refers to the neccesity of a bit more agility to cover more of the load optimally.

It can be seen from Figure 4.2 that from 70% solar fraction on, increasing N_{col} leads to only slight improvement in f_{solar} and significantly less utilization of each solar collector. The surfaces in Figures 4.1 and 4.2 are rather smooth; since, N_{series} is set to 5. Stiffer surfaces may be obtained if N_{series} is increased.

The surfaces of $Q_{supply,\ avg,\ col}$ and f_{solar} are functions of three time series: the heat load profile, the DNI and T_{amb}. The reasoning for each peak and valley becomes rather complex as it is required to keep tracking of multiple time series. To explore the effect of V_{tank} in more detail, N_{col} is kept constant as in the nominal case input set and V_{tank} is varied as 13.5 (nominal case V_{tank}), 7 and 3 m^3. The KPIs f_{supply} and f_{solar} and daily absorbed solar irradiation $Q_{abs,\ daily}$ are presented for each day in the simulation period in Figure 4.3.

It is worth mentioning that, $Q_{abs,\ daily}$ is a cumulative value, while the KPIs are functions of the actual time series.

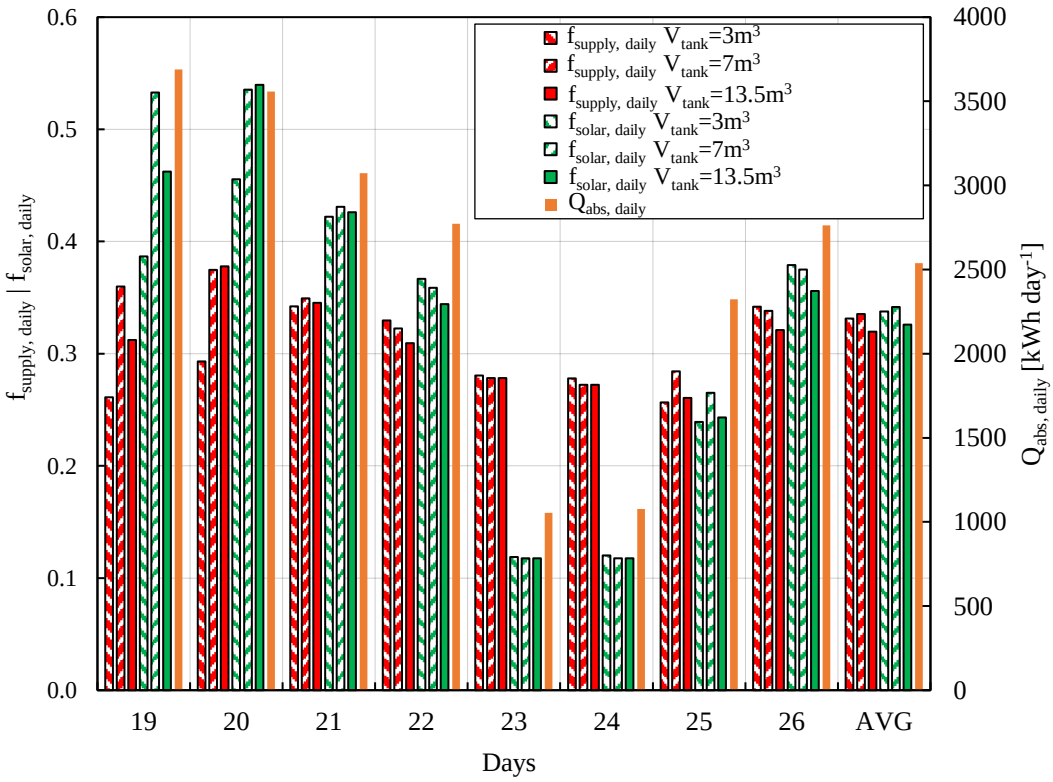

Figure 4.3. Daily calculated KPIs f_{solar} and f_{supply} for varied V_{tank} values as all other inputs are held constant at the nominal case values

It can be seen in Figure 4.3 that in the days 20th, 21st and 22nd, as $Q_{abs,\ daily}$ decreases, smaller tank volumes lead to slightly better performance in both parameters f_{supply} and f_{solar}. The series T_{tank} for each V_{tank} variant on these three days are plotted in Figure 4.4.

In Figure 4.4, on 20th July T_{tank} of smaller volume variants are observed to be greater than the greatest volume variant, leading to more heat transfer to environment. With less heat transfer to ambient, the case of V_{tank} is equal to 13.5 performs better. On 22nd; on the other hand, when slightly less DNI is available, a large storage capacity system cannot reach the target temperature due to its sluggish response.

The system with 13.5 m^3 storage tank capacity cannot compensate missing part of the 85°C load and performs slightly poorly compared to the small capacity variants. On day 21th both extremes become disadvantageous and the medium capacity system performs better under moderate DNI.

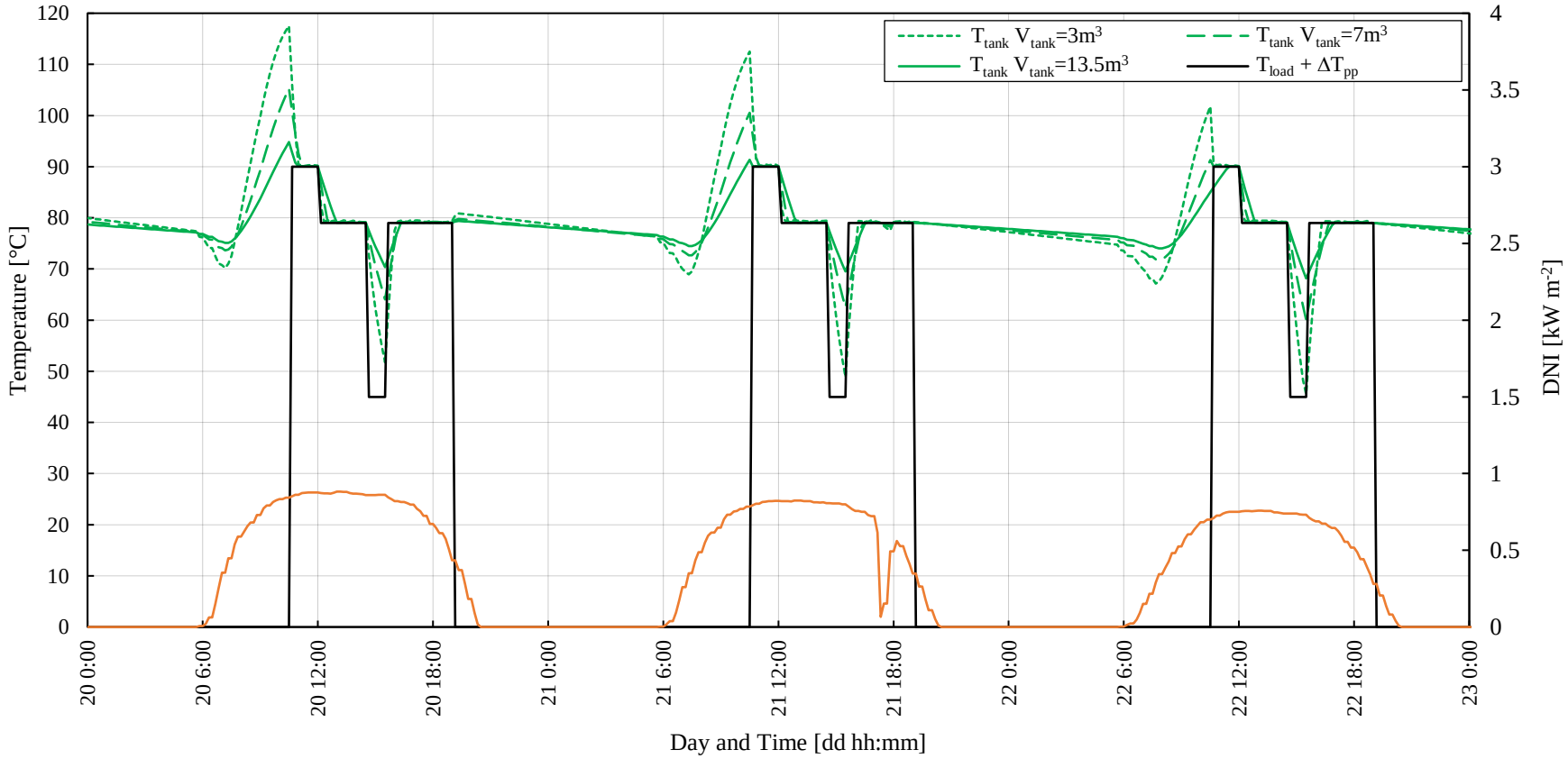

Figure 4.4. Resulting series of T_{tank} for varied V_{tank} in a three day period in which one variant's daily performance is the most superior

4.2 Impact of Collector Field Configuration – Number of Series and Parallel Connections

In this title, the impact of collector field configuration; namely, the parameters N_{series} and $N_{parallel}$ will be examined as N_{col} is kept constant at the nominal case value of 200. For this purpose, N_{series} is varied, such that Ntotal is held constant at 200, and $N_{parallel} = N_{total} / N_{series}$ as a dependent variable. N_{series} is successively set to 1, 2, 4, 5, 8, 10, 20, 25 in simulation cases; whereas, $N_{parallel}$ is set to 200, 100, 50, 40, 20, 10, 8, respectively. The resulting KPIs of f_{solar}, f_{pump}, $f_{ht\text{-}amb,col}$ and $Q_{supply,avg,col}$ are presented in Figure 4.5. Also, to see the effects of N_{series} on the temperature distribution in a series of receiver pipes, two-hour simulations are run for the same N_{series} and $N_{parallel}$ set of Figure 4.4, with 900 W m^{-2} irradiation and 0° incidence angle, under no heat load. All other inputs are held constant as in nominal case inputs and the resulting temperature distributions are presented in Figure 4.6

From Figure 4.5 it can be observed that as N_{series} is increased, f_{solar} and $Q_{supply,\ avg,\ col}$ are diminished while $f_{ht\text{-}amb,col}$ becomes greater. Focusing on Figure 4.6 for reasoning, it can be seen that as N_{series} is increased, T^0 becomes smaller while T_{end} becomes greater. The net effect of N_{series} on the average collector temperature is that the average collector temperature increases with increasing N_{series}, leading to more heat transfer from the collector side. Small T^0 also suggests small T_{tank} when N_{series} is large. On one hand, a hotter stream at a smaller flow rate, $(N_{parallel}\dot{m}_{nom})$, is pumped to the storage tank when N_{series} is large. On the other hand, a relatively cold stream at a greater flow rate, $(N_{parallel}\dot{m}_{nom})$, is pumped to the tank for small N_{series}. The net impact of N_{series} on T_{tank} is that T_{tank} ends up to be greater as N_{series} is decreased. Greater T_{tank} leads the heat load to be undertaken by solar loop for longer times. As a result, f_{solar} and $Q_{supply,\ avg,\ col}$ gets smaller with increasing N_{series} in Figure 4.5.

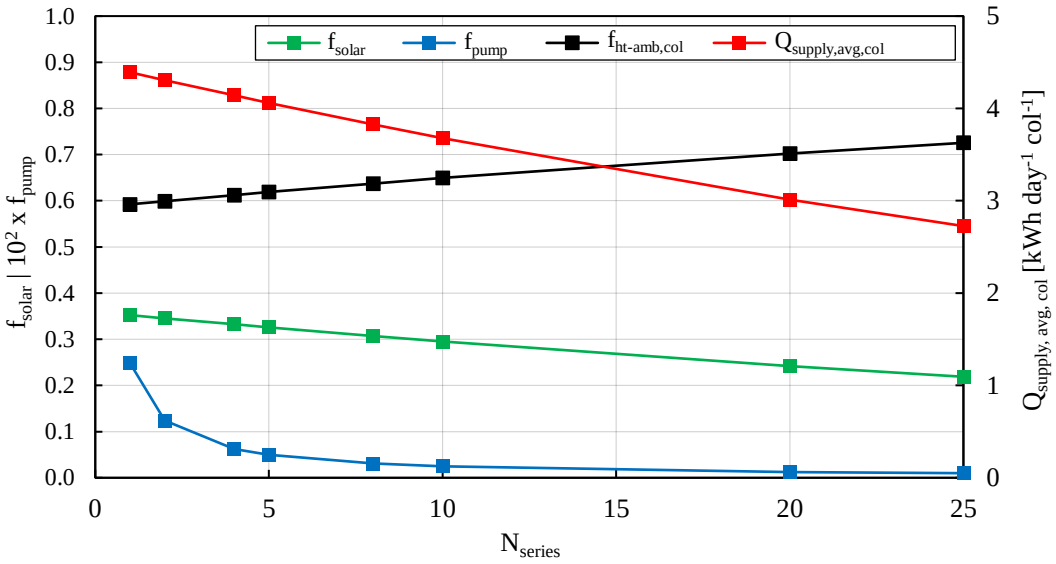

Figure 4.5. Resulting KPIs as N_{series} and $N_{parallel}$ are varied such that N_{col} and all the other inputs remains the same as in the nominal case input set

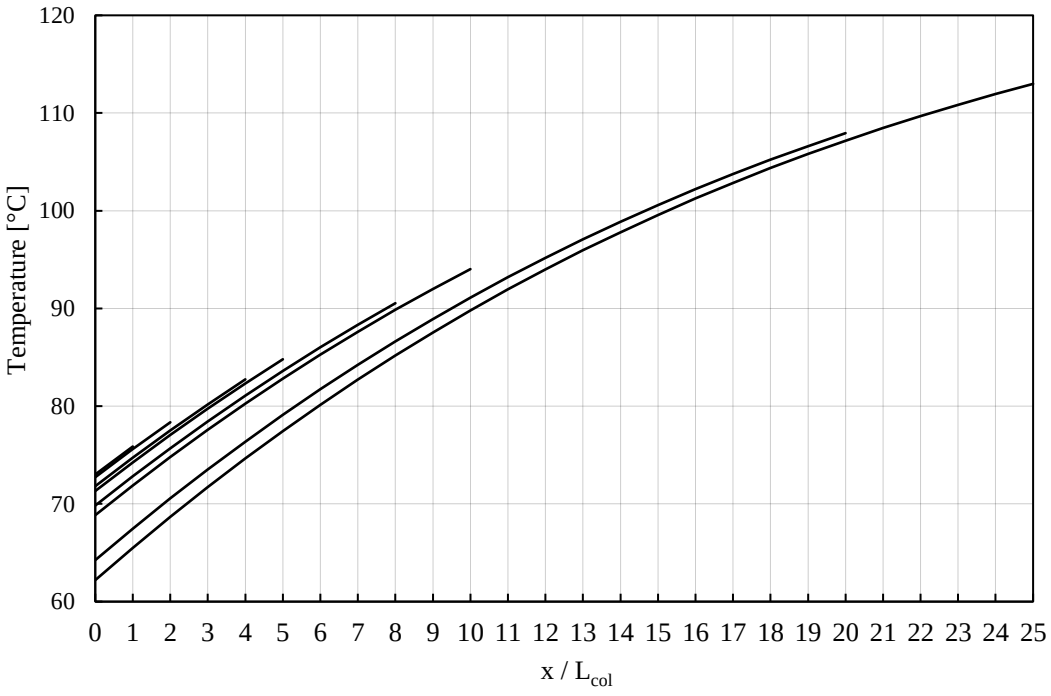

Figure 4.6. Temperature distributions for varied N_{series} values as N_{col} is kept constant after 2 hours under no load, 900 Wm^{-2} DNI and at 0° incidence angle

As N_{series} is decreased and $N_{parallel}$ is increased, the temperature in the entire SHIP plant approaches to the case of being uniformly distributed. The hypothetical case of uniform temperature distribution through the entire system would lead to the greatest solar fraction and efficiency, if the pumping power was eliminated.

In real applications; however, care must be taken when setting N_{series} to small values; as, this results in f_{pump} to increase sharply. Recalling that piping is assumed to be perfectly insulated in this study, N_{series} should be adjusted such that a significant temperature difference ($T_{col,\,avg} - T_{tank}$) is gained at each circulation around the solar loop.

4.3 Impact of Nominal Mass Flow Rate

In this section effect of the parameter $\dot{m}_{nom}$ on the system performance is explored. For this purpose, nominal case inputs are varied as presented in Table 4.1. Since CFL increases as $\dot{m}_{nom}$ is increased, Δt and Δx have to be reduced; so that, CFL remains smaller than one. Also, step sizes are adjusted to keep t_{end} and L_{sr} constant. The variations in f_{pump} and f_{solar} as a result of the $\dot{m}_{nom}$ sweep are presented in.Figure 4.7.

In, Figure 4.7 on the lower end of the $\dot{m}_{nom}$ range, f_{pump} is small. However, on the higher end of the range, for exaggerated values of $\dot{m}_{nom}$, f_{pump} reads extreme values, suggesting that W_{pump} becomes at the same order of magnitude as Q_{abs}. As a result, f_{solar} is observed to be monotonically increasing on the higher end of the $\dot{m}_{nom}$ range. It is unacceptable to increase the energy of the system by electrical pump work, so an augmented solar fraction is defined to better interpret the results of as follows:

$$f_{solar,augmented} = \frac{Q_{supply}}{Q_{load} + \frac{W_{pump}}{\eta_{th}}} \qquad \text{Eq. (4.1)}$$

The thermal load on the system is augmented by adding the electrical pump work on top of the thermal load with a heat-to-work conversion efficiency, η_{th}, of 0.25. The

KPI $f_{solar,\ augmented}$ is also plotted on Figure 4.7 and observed to have a maximum at $\dot{m}_{nom}$ is equal to 0.2 kg s^{-1}. From $\dot{m}_{nom}$ is equal to 0.2 kg s^{-1} on, $f_{solar,\ augmented}$ starts decaying as W_{pump} effects become dominant. As $\dot{m}_{nom}$ is increased up to 0.2 kg s^{-1}; however, $f_{solar,\ augmented}$ increases despite increasing f_{pump}.

Table 4.1 Varied inputs for investigating the impact of nominal mass flow rate on system performance

Symbol	$\dot{m}_{nom}$	$\dot{m}''_{nom}$	**Δt**	**N_t**	**Δx**	**N_x**	**CFL**
Unit	kg s^{-1}	kg s^{-1} cm^{-2}	sec	-	m	-	-
Values	0.02	0.004	15	46080	3.06	5	0.20
	0.03	0.006					0.30
	0.05	0.010					0.50
	0.07	0.014					0.70
	0.09	0.018					0.90
	0.11	0.022	5	138240			0.37
	0.13	0.026					0.43
	0.15	0.030					0.50
	0.20	0.039					0.67
	0.25	0.049					0.84
	0.30	0.059	3	230400			0.60
	0.40	0.079					0.80
	0.50	0.099			5.10	3	0.60
	0.60	0.118					0.72
	0.70	0.138					0.84
	0.80	0.158					0.96

To have a closer look at the $\dot{m}_{nom}$ range up to 0.2 kg s^{-1}, T_{tank} and T_{end} time series of two cases in which $\dot{m}_{nom}$ is set to 0.02 kg s^{-1} and 0.2 kg s^{-1} are plotted for the first day of the simulation in Figure 4.8. Although f_{pump} differs significantly between the two cases relative to each other, both f_{pump} values are small in absolute sense. Thus

f_{solar} and $f_{solar,\ augmented}$ are almost overlapped on top of each other in the $\dot{m}_{nom}$ range under investigation. In Figure 4.8 it is revealed that increasing $\dot{m}_{nom}$ makes the series T_{tank} and T_{end} come closer to each other. If the pumping power was to be eliminated, the series T_{tank} and T_{end} would merge on the line of lumped solution. From this point of view, increasing $\dot{m}_{nom}$ has a similar impact as increasing $N_{parallel}$ (and decreasing N_{series} such that N_{col} is kept constant).

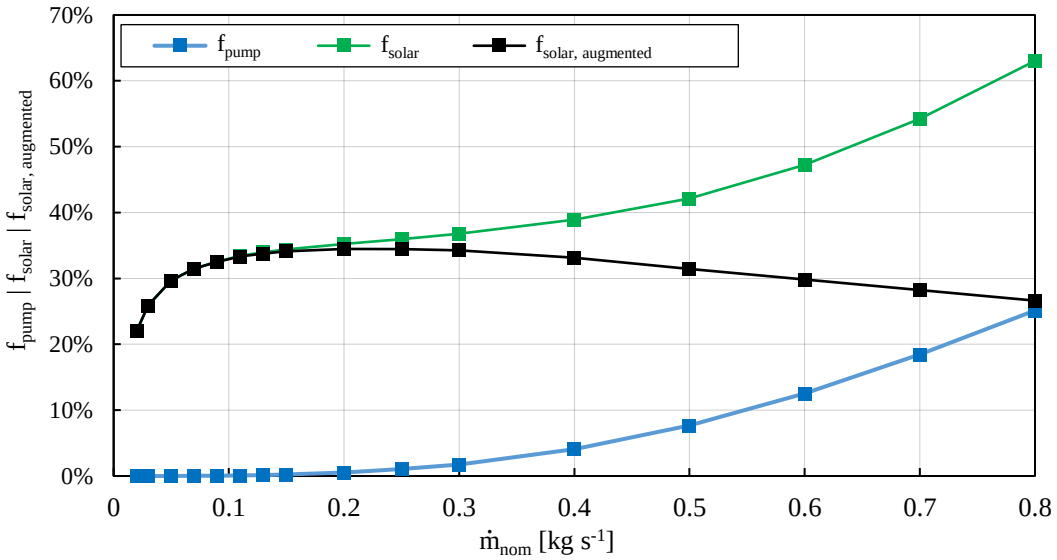

Figure 4.7. Resulting KPIs f_{pump}, f_{solar}, $f_{solar,\ augmented}$ of $\dot{m}$ sweep as Δt, Δx, N_t and N_x are adjusted to keep CFL under unity and all other inputs are held constant at nominal values

The case of series T_{tank} and T_{end} approaching to the lumped solution is desirable as this results in a higher T_{tank}. That delays T_{tank} dropping below (T_{load} + ΔT_{pp}) and results in a smaller T_{end} leading to less heat transfer to ambient.

As $\dot{m}_{nom}$ is increased, the series T_{tank} and T_{end} first approach to each other around the lumped solution. When $\dot{m}_{nom}$ is kept increasing, the series T_{tank} and T_{end} approach to each other even more; but, depart from the lumped solution as the pumping power effects are becoming dominant. Significant enthalpy gain is

observed in HTF between the inlet and the exit of the pump, due to the immense pumping power. To conclude, it is recommended to set $\dot{m}_{nom}$ as high as possible, keeping an eye on the pumping power.

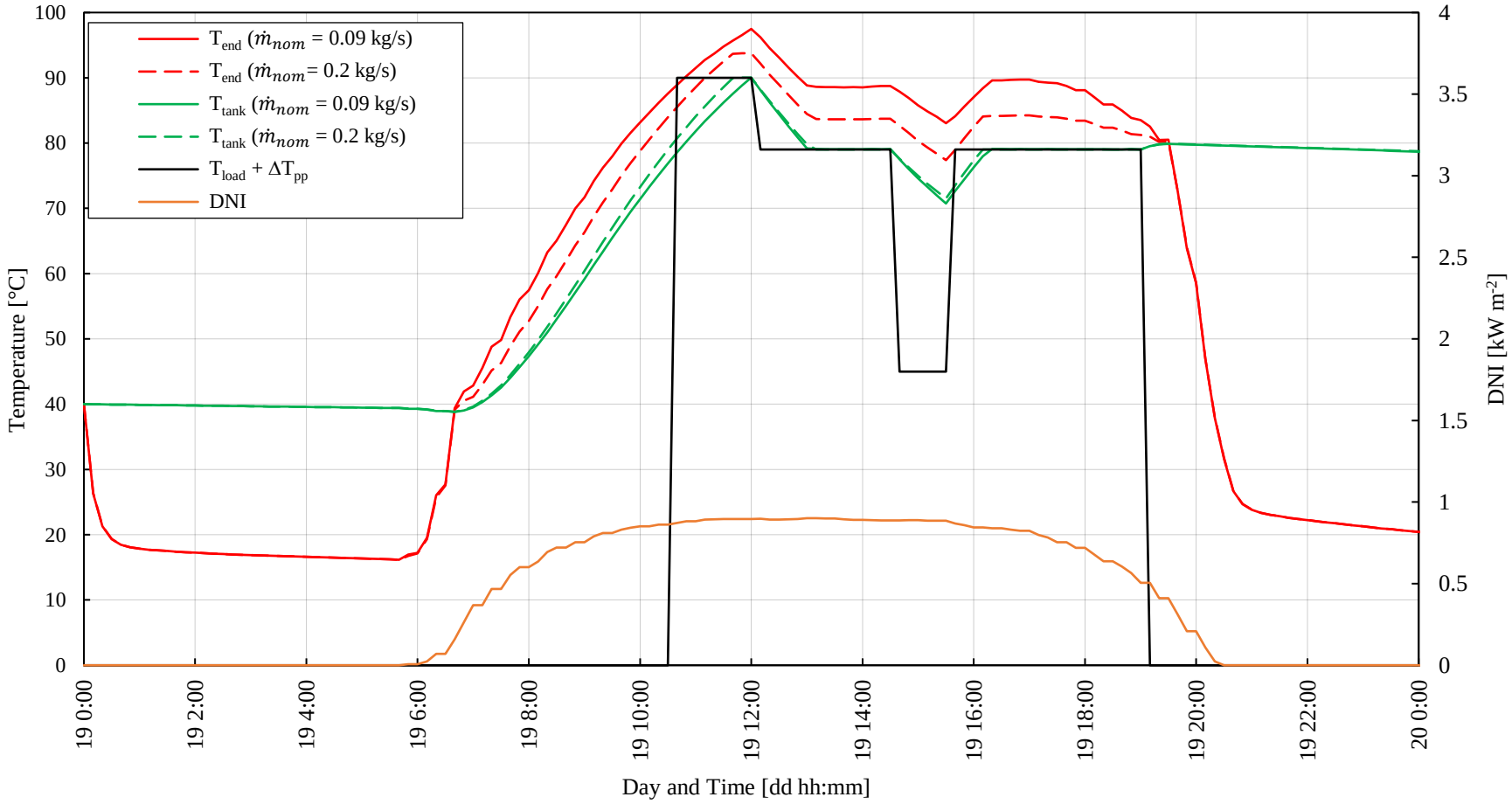

Figure 4.8. Resulting series of T_{tank} and T_{end} as $\dot{m}_{nom}$ variants of the nominal case and the $\dot{m}_{nom}$ at which $f_{solar,\ augmented}$ is maximum

4.4 Suggested System and the Control Strategy

In this headline, options for improving performance by modifying the plant architecture and taking advantage of control are explored. The suggestions are based on the conclusions drawn from the parametric analysis and the pitfalls of the modeled system.

In the present model the heat load is assumed to be satisfied by the storage tank as long as the condition of equation 2.17 is met, independent of T_{tank}. Furthermore, pump1 and the process fluid pump, i.e., the milk pump speeds are modulated to control $T_{pf,\ out}$. In the real case; however, this level of flexibility might not be achieved. Therefore, it is desirable to hold T_{tank} stable at a preset temperature. Such that the HEX is designed accordingly and pump1 and the process fluid pump operate at constant speeds.

Interpreting the results in the parametric analysis part, it can be seen that temperature control of T_{tank} by flow rate modulation in the present system is not possible. Any modulation of $\dot{m}$ will result in T_{tank} to eventually increase. It would be possible to control T_{tank} by allowing the controller to manipulate the fill and drain valves, referring to V_{tank} modulation. According to the parametric analysis, it is foreseen that variable tank volume will only lead to very slim improvement in performance. Alternatively, stabilizing T_{end} by adjusting $\dot{m}$ and sending the flow directly to the HEX may be considered. Through this alternative; although, a constant T_{end} is obtained, stable operation of HEX cannot be achieved due to the variable $N_{parallel}\dot{m}$. Moreover, a great pressure drop in HEX is expected for collector fields that have numerous parallel connections. The alternative of stabilizing T_{end} and feeding the flow directly to the HEX requires many collectors to be in series rather than parallel, though.

It is revealed in the previous sections that most of the heat transfer to ambient in the system is from the collector side. In the current system, even if T_{tank} is reached to elevated temperatures, the HTF in the tank is continued to be circulated through the

solar loop (as long as the condition in equation 2.10 is satisfied), leading to a high $T_{avg,\,col}$; thus, heat transferred to surroundings is increases. The hot stream from the collector field is mixed with the relatively cold HTF in the storage tank, increasing entropy for no apparent reason. To prevent the stated drawbacks of the current single-tank system, the two-tank system illustrated in Figure 4.9 is suggested with PI T_{end} control by manipulated $\dot{m}$. The suggested system starts the day with an empty the hot-tank. As the sun rises, the pump is operated at a speed that sets T_{end} to slightly higher than ($T_{load} + \Delta T_{pp}$) and the HTF flow at the collector outlet is directed to the hot tank. In some sense, this could be regarded as storing thermal energy not in the sensible heat, but in the volume. The optimum values for N_{series} and $N_{parallel}$ are expected to read different values for the two-tank system. In order to achieve the setpoint temperature at the collector field outlet, N_{series} would be increased significantly. As stratification is not expected in constant temperature tanks, the lumped model conserves its validitiy.

HTF level in the hot tank rises until the heat load is demanded. When the heat load is demanded, HTF from the hot tank is pumped to the HEX. From the HEX outlet either the stream is directed to the cold tank or it is mixed with the stream from the cold tank in a mixing chamber. The two-tank system also offers smoother integration of the auxiliary heater to the solar system. The stream from the auxiliary heater can be directed and stored in the hot-tank.

In Figure 4.10, the PI control strategy with a proportional constant, K_p of 0.5 and the integral constant K_i of 10^{-3} is demonstrated in action as it is stabilizing T_{end} at the preset value of ($T_{load} + \Delta T_{pp}$) under varied DNI conditions. Manipulated $\dot{m}$ is forced to be in the range $(0.1)\dot{m}_{nom} \leq \dot{m}_{PI} \leq (2.5)\dot{m}_{nom}$. In the simulation resulted in Figure 4.10, solar incidence angle is set to 0°. It is observed that the steady state error is prevented by the integral term. Furthermore, the sharp peak is observed as the setpoint value is suddenly changed due to the proportional term. The overall behavior of the PI controller is as expected and sufficient to control the thermal system under investigation.

While the control strategy discussed in the previous paragraph leads to improved performance it could further be advanced by introducing a cascaded T_{tank} control that adjust the setpoint of T_{end}. As a result, the heat transfer from the tank to the environment can be better compensated. Cascade control also enables pumping relatively cold HTF from the cold-tank if T_{tank} is overshoot. To introduce more flexibility to the controller, dynamic collector field configuration can also be implemented using electrically controlled three-way-valves.

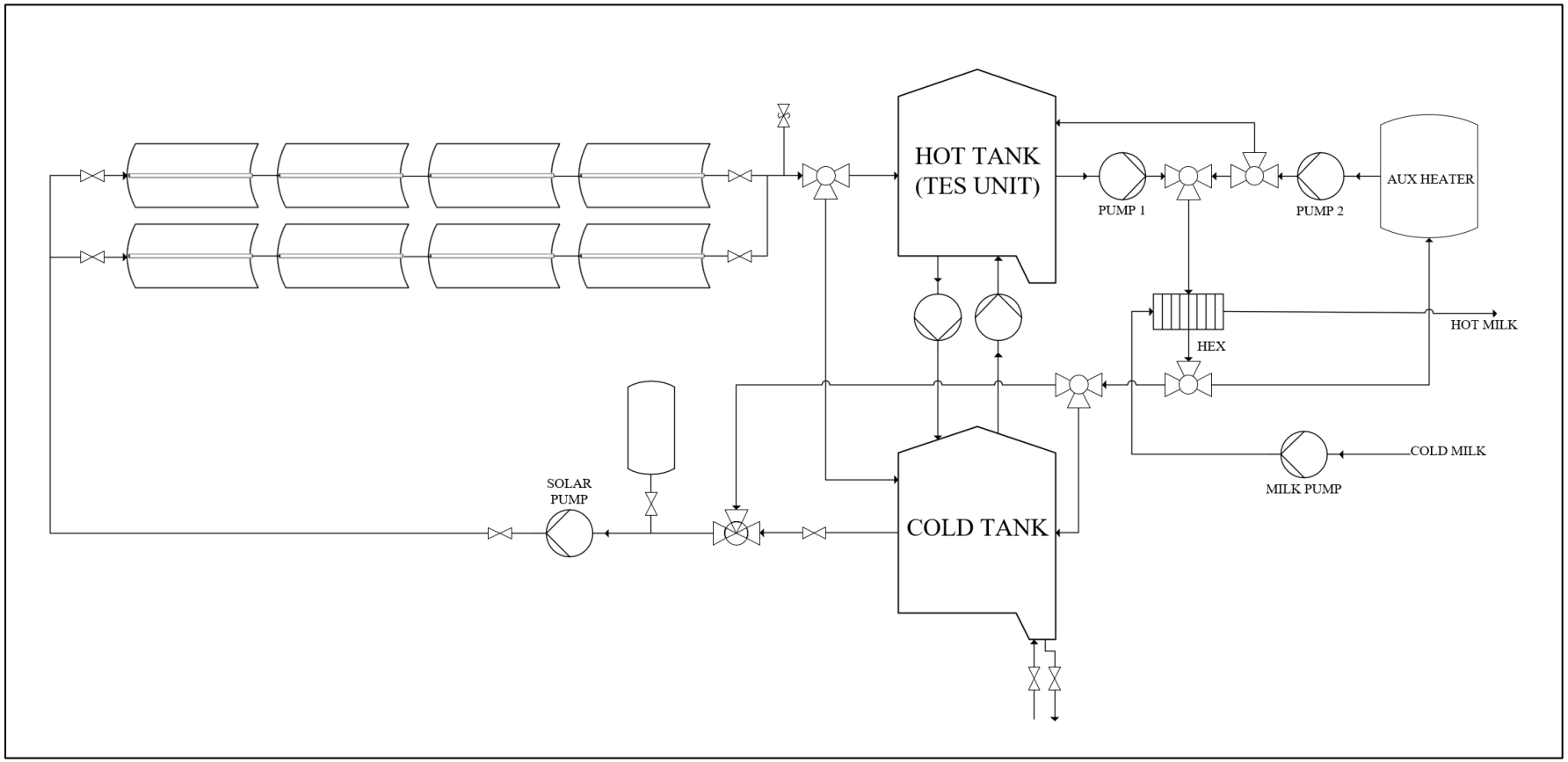

Figure 4.9. Suggested two-tank architecture for the milk pasteurization SHIP plant

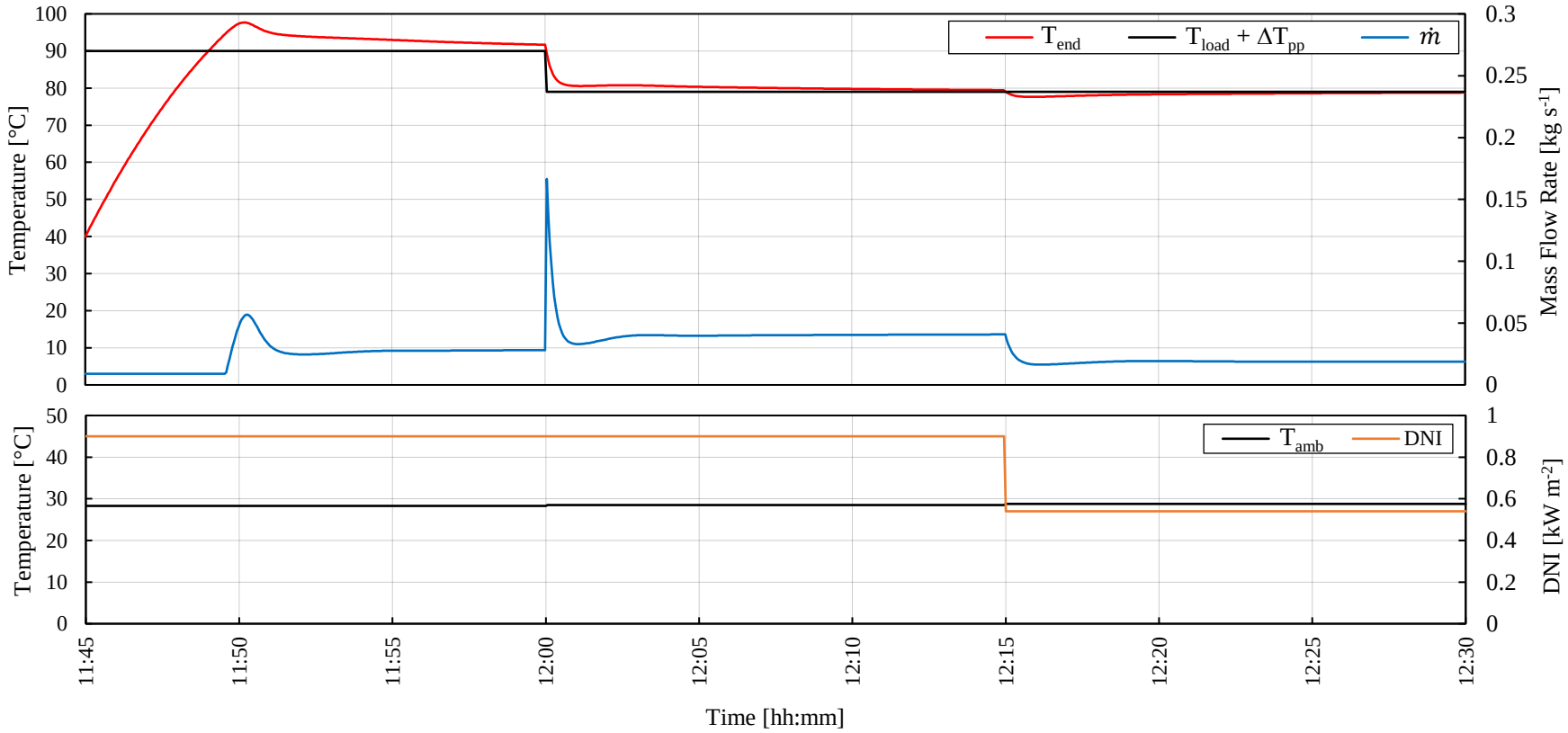

Figure 4.10. Demonstration of PI control of T_{end} by mass flow rate modulation (Horizontal gridlines are aligned).

CHAPTER 5

CONCLUSION

In this study, several solar heat integration steps into a milk pasteurization process are covered. The procedure starts with the target heat load profile that is shared with METU by AEE-INTEC. Time dependency of the load temperature is addressed with modeling and simulation of a preliminary system with a single-tank TES with real meteorological data, using the developed simulation tool. For the preliminary system, PTC technology is considered as the solar collector, pressurized water is selected as HTF and the HTF also acts as the energy storage medium. Modeling of individual components are presented and discretized for the FVM solution. An on-off control strategy is adapted to the single-tank system. The solar pump is turned off if solar heat absorbed by the HTF is less than the heat transfer from HTF to the environment. A 1D dynamic PTC model is used; as it is desirable to obtain the transient plant response for PI control. 1D model also gives more accurate performance estimation. Using an auxiliary, 0D transient simulation tool, nominal case inputs are systematically specified. The actual simulation tool's inputs, outputs, data and program flow are introduced. Simulation results of the nominal case are presented, mesh independence and energy balance are checked. The PTC model is validated by comparison with references [64,65].

In simulation results chattering is observed when the solar pump is turned on, because the relatively hot HTF from the tank is immediately filled into the receiver pipe. That leads to heat transfer to surroundings to suddenly take place at a higher rate, and the pump is turned off in the next time step. Chattering is not observed when turning off the solar pump as solar radiation diminishes. Nominal case simulation results also indicated that the work input to the solar pump is negligibly small, as expected, for the selected mass flow of 0.09 kg s^{-1}. While 95% of the heat transfer to the environment is from the collector side, 5% is from the storage tank.

The simulation revealed that with 200 collectors, corresponding to a total collector area of 673 m^2, and a storage tank capacity of 13.51 m^3, 33% of the process heat load is covered by solar heat in the summer season. If the same load profile was defined for the winter season, a smaller solar fraction is expected in the winter time due to smaller DNI and solar incidence angles. In this case, the solar system may be used for pre-heating.

A parametric analysis is conducted to explore the effects of number of collectors and storage tank volume together, number of series and parallel connections and mass flow rate. Results showed that more storage and collectors are simultaneously needed to increase the solar fraction. Also, smaller tank volumes leading to a more agile system, are slightly advantageous in cloudy days. Daily heat supplied to the process per collector is maximized if only the 40°C portion of the load is covered. It is observed that increasing the number of collectors does not lead to significant improvement in solar fraction from around 70% on. This can be generalized as the coldest portion of the load is the section where maximum collector utilization is observed. The parametric study outcomes end up to be consistent with the literature.

The impact of increasing the number of series connections by keeping the total number of collectors constant results in smaller solar fraction, but less pumping power. This was an expected outcome, as the number of series connections are increased, the average temperature of the HTF in collector field increases; as a result, heat transfer to the surroundings increase. It is suggested to keep the number of collectors in series small, such that the pumping power is reasonable and an increase in HTF temperature is ensured in the collector field.

The effect of increasing the mass flow rate results in greater solar fraction and heat supplied by each collector, until the fairly non-linear effects of pumping power lead to poor performance. In the range that pump work is negligibly small, as mass flow rate become greater, temperature distribution in the SHIP plant approaches to the hypothetical case of uniform temperature distribution.

By the parametric analysis results, it is concluded that the primary pitfall of the single-tank architecture is that the hot stream of HTF from the collector field is mixed with the relatively cold HTF in the TES unit. The tank temperature cannot be controlled by mass flow rate modulation unless its volume is varied. Continuing the integration process holistically, a two-tank architecture is suggested with variable speed solar pump. PI control of the temperature at the collector field exit by flow rate modulation is suggested as the primary strategy. The control strategy is demonstrated in the present study.

Simulation and performance estimation of the two-tank system for a time dependent load profile can be studied in a future work. Also, stratified tank model, HEX model, delays in piping can be implemented in the following versions of the existing simulation tool. Including the receiver pipe walls to the discretized domain and taking the circumferential heat flux variation into account are among the items in the development list. It would also be beneficial to study the non-dimensional version of the present model. The MS Excel VBA, using a single thread for calculations, significantly increases the execution time of simulations. So, the macro will only be used to enter formulas to the cells in the upcoming versions.

In some cases, solar energy may be concerned to supply both the electricity and the heat demand of a facility. In these cases low-temperature SHIP provides great opportunity to be cogenerated with; for example, an organic rankine cycle (ORC). If cooling is also demanded for the industrial process, trigeneration is possible using solar heat in an absorption cooling cycle. System design, modeling, and simulation of such combinations are also suggested as future work.

REFERENCES

[1] Patil, P. G., and Alok S., 1984, "State-Of-The-Art Of Solar Thermal Industrial Process Heat Technologies For Use In Developing Countries" pp. 577–583.

[2] Farjana, S. H., Huda, N., et al. 2018, "Solar Process Heat in Industrial Systems – A Global Review," Renewable and Sustainable Energy Reviews, **82**(June 2017), pp. 2270–2286.

[3] "World Energy Statistics 2016, Online Tables" [Online]. Available: www.iea.org/statistics/, [Accessed: 02-09-2019].

[4] Hachicha, A. A., Yousef, B. A. A., et al. 2019, "A Review Study on the Modeling of High-Temperature Solar Thermal Collector Systems," Renewable and Sustainable Energy Reviews, **112**(June), pp. 280–298.

[5] Kalogirou, S., 2003, "The Potential of Solar Industrial Process Heat Applications," Applied Energy, **76**(4), pp. 337–361.

[6] Epp, B., and Oropeza, M., 2017, *Solar Heat for Industry (Solar Payback)*.

[7] Sharma, A. K., Sharma, C., et al. 2017, "Solar Industrial Process Heating: A Review," Renewable and Sustainable Energy Reviews, **78**, pp. 124–137.

[8] Silva, R., Berenguel, M., et al. 2014, "Thermo-Economic Design Optimization of Parabolic Trough Solar Plants for Industrial Process Heat Applications with Memetic Algorithms," Applied Energy, **113**, pp. 603–614.

[9] Hess, S., and Oliva, A., 2012, "SO-PRO Solar Process Heat," Energiesparverband, p. 27.

[10] Lovegrove, K., and Stein, W., 2012, *Concentrating Solar Power Technology*.

[11] Atkins, M. J., Walmsley, M. R. W., et al. "Integration of Solar Thermal for Improved Energy Efficiency in Low-Temperature-Pinch Industrial Processes," Energy, **35**(5), pp. 1867–1873.

[12] Baniassadi, A. M., and Amidpour, M., 2015, "A New Method for Optimization of Solar Heat Integration and Solar Fraction Targeting in Low Temperature Process Industries," Energy, **90**, pp. 1674–1681.

[13] Cotrado, M., Dalibard, A., et al. 2014, "Design, Control and First Monitoring Data of a Large Scale Solar Plant at the Meat Factory Berger, Austria," *Energy Procedia*, Elsevier Ltd, pp. 1144–1151.

[14] Baniassadi, A., Momen, M, et al. 2018, "Modeling and Design of Solar Heat Integration in Process Industries with Heat Storage," Journal of Cleaner Production, **170**, pp. 522–534.

[15] Walmsley, T. G., Walmsley, M. R. W., et al. "Integration Options for Solar Thermal with Low Temperature Industrial Heat Recovery Loops," Energy, **90**, pp. 113–121.

[16] Muster, B., Hassine, I., et al. 2015, "Solar Process Heat for Production and Advanced Applications: Integration Guideline," IEA SHC Task 49, (February)

[17] Yılmaz, İ. H., and Mwesigye, A., 2018, "Modeling, Simulation and Performance Analysis of Parabolic Trough Solar Collectors: A Comprehensive Review," Applied Energy, **225**(February), pp. 135–174.

[18] Therminol Inc., *Technical Data Sheet VP-1*.

[19] Wang, Z., 2019, "General Design of a Solar Thermal Power Plant," *Design of Solar Thermal Power Plants*, pp. 117–224.

[20] Dudley, V. E., Kolb, G. J., et al. 1994, *Test Results SEGS LS-2 Solar Collector*.

[21] Dudley, V. E., and Workhoven, R. M., 1982, *Performance Testing of the ACUREX Solar Collector Model 3001-03*.

[22] Dudley, V. E., Evans, L. R., and Matthews, C. W., 1995, *Test Results IST PTC*.

[23] Padilla, R. V., 2011, "Simplified Methodology for Designing Parabolic Trough Solar Power Plants."

[24] García-Valladares, O., and Velázquez, N., 2009, "Numerical Simulation of Parabolic Trough Solar Collector: Improvement Using Counter Flow Concentric Circular Heat Exchangers," International Journal of Heat and Mass Transfer, **52**(3–4), pp. 597–609.

[25] Padilla, R. V., Demirkaya, G., et al. 2011, "Heat Transfer Analysis of Parabolic Trough Solar Receiver," Applied Energy, **88**(12), pp. 5097–5110.

[26] Kalogirou, S. A., 2012, "A Detailed Thermal Model of a Parabolic Trough Collector Receiver," Energy, **48**(1), pp. 298–306.

[27] Yang, S., Sensoy, T. S., and Ordonez, J. C., 2018, "Dynamic 3D Volume Element Model of a Parabolic Trough Solar Collector for Simulation and Optimization," Applied Energy, **217**, pp. 509–526.

[28] Cheng, Z. D., He, Y. L., et al., 2012, "Numerical Simulation of a Parabolic Trough Solar Collector with Nonuniform Solar Flux Conditions by Coupling FVM and MCRT Method," Solar Energy, **86**(6), pp. 1770–1784.

[29] Gong, G., Huang, X., et al., 2010, "An Optimized Model and Test of the China's First High Temperature Parabolic Trough Solar Receiver," Solar Energy, **84**(12), pp. 2230–2245.

[30] Forristall, R., 2003, *Heat Transfer Analysis and Modeling of a Parabolic Trough Solar Receiver Implemented in Engineering Equation Solver*.

[31] Qu, M., Archer, D. H., and Yin, H., 2007, "A Linear Parabolic Trough Solar Collector Performance Model," Proceedings of the Energy Sustainability Conference 2007, pp. 663–670.

[32] Marcos, A., Siqueira, D. O., et al., 2014, “Heat Transfer Analysis and Modeling of a Parabolic Trough Solar Collector: An Analysis,” Energy Procedia, **57**(31), pp. 401–410.

[33] Gnielnski, V., 1976, “New Equations for Heat and Mass Transfer in Turbulent Pipe and Channel Flow,” International Chemical Engineering, **562**(2), pp. 359–363.

[34] Ratzel, A. C., Hickox, C. E., and Gartling, D. K., 1979, “Techniques For Reducing Thermal Conduction And Natural Convection Heat Losses In Annular Receiver Geometries,” J Heat Transfer Trans ASME, **101**(1), pp. 108–113.

[35] Hollands, K. G. T., Raithby, G. D., and Konicek, L., 1975, “Correlation Equations for Free Convection Heat Transfer in Horizontal Layers of Air and Water,” International Journal of Heat and Mass Transfer, **18**(7–8), pp. 879–884.

[36] Churchill, S. W., and Chu, H. H. S., 1975, “Correlating Equations for Laminar and Turbulent Free Convection from a Horizontal Cylinder,” International Journal of Heat and Mass Transfer, **18**(9), pp. 1049–1053.

[37] Žukauskas, A., 1972, “Heat Transfer from Tubes in Crossflow,” Advances in Heat Transfer, **8**(C), pp. 93–160.

[38] Camacho, E. F., Berenguel, M., Rubio, F. R., and Martínez, D., 2012, *Control of Solar Energy Systems*, Springer London, London.

[39] Camacho, E. F., Berenguel, M., and Rubio, F. R., 1997, *Advanced Control of Solar Plants*, Springer London, London.

[40] Bocci, E., Villarini, M., et al., 2012, “Modeling Small Scale Solar Powered ORC Unit for Standalone Application,” Mathematical Problems in Engineering, **2012**.

[41] Bayer, Ö., and Uzgoren, E., 2018, “Comparison of Dynamic PTC Thermal Models Using Semi-Analytical and Finite Volume Methods,” Environmental Progress and Sustainable Energy, **37**(3), pp. 1191–1200.

[42] Wu, Z., Li, S., et al., 2014, “Three-Dimensional Numerical Study of Heat Transfer Characteristics of Parabolic Trough Receiver,” Applied Energy, **113**, pp. 902–911.

[43] Uygur, S., 2021, “Detailed Simulations Of Parabolic Trough Collector For Investigating Enhancement Of Heat Transfer To Absorber Tube Flow.”

[44] Kumaresan, G., Sridhar, R., and Velraj, R., 2012, “Performance Studies of a Solar Parabolic Trough Collector with a Thermal Energy Storage System,” Energy, **47**(1), pp. 395–402.

[45] Powell, K. M., and Edgar, T. F., 2012, “Modeling and Control of a Solar Thermal Power Plant with Thermal Energy Storage,” Chemical Engineering Science, **71**, pp. 138–145.

[46] Silva, R., Pérez, M., and Fernández-Garcia, A., 2013, “Modeling and Co-Simulation of a Parabolic Trough Solar Plant for Industrial Process Heat,” Applied Energy, **106**, pp. 287–300.

[47] Stuber, M. D., 2018, “A Differentiable Model for Optimizing Hybridization of Industrial Process Heat Systems with Concentrating Solar Thermal Power,” Processes, **6**(7).

[48] Villarini, M., Bocci, E., et al., 2013, “Technical-Economic Analysis of an Innovative Small Scale Solar Thermal - ORC Cogenerative System,” Lecture Notes in Computer Science (including subseries Lecture Notes in Artificial Intelligence and Lecture Notes in Bioinformatics), **7972**(PART 2), pp. 271–287.

[49] Bartali, R., Bayer, Ö., et al., 2020, “Water Sludge Drying : Modelling of a Solar Thermal Plant for a Solar Vacuum Dryer,” *EuroSun 2020*, International Solar Energy Society.

[50] Bartali, R., Christodoulaki, R., et al., 2020, “Decarbonization of Industrial Processes: Technologies, Applications and Perspectives of Low- Temperature Solar Heat (80-150°C),” *EuroSun 2020*, International Solar Energy Society.

[51] Epp, B., 2021, “German University Offers New Tool to Display Factory Heat Loads”[Online]. Available: http://www.solarthermalworld.org/news/german-university-offers-new-tool-display-factory-heat-loads, Accessed: [07-11-2021].

[52] Meaburn, A., and Hughes, F. M., 1995, “Pre-Scheduled PID Control of a Solar Thermal Power Plant,” Transactions of the Institute of Measurement and Control, **17**(3), pp. 132–142.

[53] Johansen, T. A., and Storaa, C., 2002, “Energy-Based Control of a Distributed Solar Collector Field,” Automatica, **38**(7), pp. 1191–1199.

[54] Juuso, E. K., 2005, “Modelling and Control of a Solar Thermal Power Plant,” *IFAC Proceedings Volumes (IFAC-PapersOnline)*, IFAC Secretariat, pp. 368–373.

[55] Camacho, E. F., Rubio, F. R., et al., 2007, “A Survey on Control Schemes for Distributed Solar Collector Fields. Part I: Modeling and Basic Control Approaches,” Solar Energy, **81**(10), pp. 1240–1251.

[56] Camacho, E. F., Rubio, F. R., et al. 2007, “A Survey on Control Schemes for Distributed Solar Collector Fields. Part II: Advanced Control Approaches,” Solar Energy, **81**(10), pp. 1252–1272.

[57] Pietruschka, D., Fedrizzi, R., et al. 2012, “Demonstration of Three Large Scale Solar Process Heat Applications with Different Solar Thermal Collector Technologies,” *Energy Procedia*, Elsevier Ltd, pp. 755–764.

[58] Gallego, A. J., and Camacho, E. F., 2012, “Adaptative State-Space Model Predictive Control of a Parabolic-Trough Field,” Control Engineering Practice, **20**(9), pp. 904–911.

[59] Gallego, A. J., Fele, F., Camacho, E. F., and Yebra, L., 2013, “Observer-Based Model Predictive Control of a Parabolic-Trough Field,” Solar Energy, **97**, pp. 426–435.

[60] Fontalvo, A., Garcia, J., Sanjuan, M., and Padilla, R. V., 2014, “Automatic Control Strategies for Hybrid Solar-Fossil Fuel Power Plants,” Renewable Energy, **62**, pp. 424–431.

[61] Xu, X., Yuan, Y., and Dubljevic, S., 2017, “Optimal Control of a Distributed Solar Collector Field,” *Proceedings of the American Control Conference*, Institute of Electrical and Electronics Engineers Inc., pp. 1821–1826.

[62] Li, L., Li, Y., and He, Y. L., 2020, “Flexible and Efficient Feedforward Control of Concentrating Solar Collectors,” Applied Thermal Engineering, **171**(September 2019).

[63] Kannaiyan, S., Bokde, N. D., and Geem, Z. W., 2020, “Solar Collectors Modeling and Controller Design for Solar Thermal Power Plant,” IEEE Access, **8**, pp. 81425–81446.

[64] Bubolz, K., 2014, “Systeme Hyperbolischer Partieller Differentialgleichungen : Temperaturstabilisierung in Parabolrinnensolarkraftwerken.”

[65] Noureldin, K., González-Escalada, L. M., et al., 2016, “Modelling and Optimization of Transient Processes in Line Focusing Power Plants with Single-Phase Heat Transfer Medium Virtual Solar Field-An Opportunity to Optimize Transient Processes in Line-Focus CSP Power Plants AIP Conference Modelling and Optimization,” **1734**, p. 160005.

[66] Buzás, J., 2009, “Block-Oriented Modeling Of Solar Thermal Systems.”

[67] Tilahun, F. B., Bhandari, R., and Mamo, M., 2019, “Design Optimization and Control Approach for a Solar-Augmented Industrial Heating,” Energy, **179**, pp. 186–198.

[68] Abikoye, B., Čuček, L., et al., 2019, “Integrated Design for Direct and Indirect Solar Thermal Utilization in Low Temperature Industrial Operations,” Energy, **182**, pp. 381–396.

[69] Buzás, J., and Kicsiny, R., 2014, “Transfer Functions of Solar Collectors for Dynamical Analysis and Control Design,” Renewable Energy, **68**, pp. 146–155.

[70] Kicsiny, R., 2015, “Transfer Functions of Solar Heating Systems for Dynamic Analysis and Control Design,” Renewable Energy, **77**, pp. 64–78.

[71] Kicsiny, R., and Varga, Z., 2013, “Real-Time Nonlinear Global State Observer Design for Solar Heating Systems,” Nonlinear Analysis: Real World Applications, **14**(2), pp. 1247–1264.

[72] Hess, S., Oliva, A., Hermann, M., Stryi-Hipp, G., and Hanby, V., 2011, “Solar Process Heat-System Design for Selected Low-Temperature Applications in the Industry,” 30th ISES Biennial Solar World Congress 2011, SWC 2011, **5**(June 2016), pp. 3451–3462.

[73] Franco, A., 2020, “Methods for the Sustainable Design of Solar Energy Systems for Industrial Process Heat,” Sustainability (Switzerland), **12**(12).

[74] Anastasovski, A., Rašković, P., et al., 2020, “A Systematisation of Methods for Heat Integration of Solar Thermal Energy in Production Processes: A Review,” Journal of Sustainable Development of Energy, Water and Environment Systems, **8**(2), pp. 410–437.

[75] Garg, H. P., and Garg, H. P., 1987, “Solar Energy for Industrial Process Heat,” *Advances in Solar Energy Technology*, Springer Netherlands, pp. 103–167.

[76] Schmitt, B., 2016, “Classification of Industrial Heat Consumers for Integration of Solar Heat,” *Energy Procedia*, pp. 650–660.

[77] STS-Med, 2016, *Concentrated Solar Thermal Energy Systems Handbook*.

[78] “SHIP Plants Database” [Online]. Available: http://ship-plants.info/. [Accessed: 14-Dec-2021].

[79] “Inventive Power Power Trough 110” [Online]. Available: https://inventivepower.com.mx/english/power-trough-110/. [Accessed: 14-Dec-2021].

[80] Beckman, W. A., 2013, “Solar Engineering of Thermal Processes.”

[81] Kalogirou, S. A., 2014, *Solar Energy Engineering. Processes and Systems*, Elsevier.

[82] Colebrook, C. F., 1939, “Turbulent Flow In Pipes, With Particular Reference To The Transition Region Between The Smooth And Rough Pipe Laws.,” Journal of the Institution of Civil Engineers, **11**(4), pp. 133–156.

[83] Mawire, A., and Taole, S. H., 2013, “Heat Loss Estimation in a Small Vertical Cylindrical Stratified Oil Storage Tank,” Proceedings of the 21st Conference on the Domestic Use of Energy, DUE 2013, pp. 107–113.

[84] Gelaro, R., McCarty, W., et al., 2017, “The Modern-Era Retrospective Analysis for Research and Applications, Version 2 (MERRA-2),” Journal of Climate, **30**(14), pp. 5419–5454.